Supporting Information

Solvent-Free *N*–Alkylation and Dehydrogenative Coupling Catalysed by a Highly Active Pincer–Nickel Complex

Vinay Arora,[†a] Moumita Dutta,[†a] Kanu Das,[a] Babulal Das,[a] Hemant Kumar Srivastava,*[a,b] and Akshai Kumar *[a,c]

[†]*Equal contribution*

Email: akshaikumar@iitg.ac.in, hemantkrsri@gmail.com

[a]*Department of Chemistry, Indian Institute of Technology Guwahati, Guwahati – 781039, Assam, India.*
[b]*National Institute of Pharmaceutical Education and Research Guwahati, Guwahati – 781030, Assam, India.*
[c] *Center for Nanotechnology, Indian Institute of Technology Guwahati, Guwahati – 781039, Assam, India.*

Table of Contents

1. X-ray Analysis

Table S1. Crystal structure and refinement parameters of (^{iPr2}NNN)$NiCl_2(H_2O)$

Complex	**(^{iPr2}NNN)$NiCl_2(H_2O)$**
Empirical formula	C_{13} H_{21} Cl_2 N_3 Ni O
Formula weight	364.94
Crystal size (mm^3)	0.38 × 0.26 × 0.18
Space group	*C2/c*
a (Å)	18.487(3)
b (Å)	11.214(3)
c (Å)	8.6528(15)
α (deg)	90.00
β (deg)	116.901(8)
γ (deg)	90.00
V ($Å^3$)	1599.7(6)
Z	4
$\rho_{calc.}$ ($g \cdot cm^{-3}$)	1.515
μ (M_0 Kα)(mm^{-1})	1.545
F(000)	760
T(K)	296(2)
Range of indices	-21, 21; -13, 13; -10, 10
No. of reflections collected	25122
Unique reflections	1408
Completeness to 2θ	100.00
R_{int}	0.0531
Data / restraints / parameters	1408 / 0 / 99
Goodness-of-fit	1.115
$R_1[I \geq 2\sigma(I)]$	0.0534
wR_2 $[I \geq 2\sigma(I)]$	0.1471
R_1 (all data)	0.0905
wR_2 (all data)	0.1737
Δ_r(max, min) e $Å^{-3}$	0.666, -0.648

Table S2. Selected Bond lengths and angles around metal (Ni) centre

(^{iPr2}NNN)$NiCl_2(H_2O)$			
Ni-N-Ar (Å)	2.008(6)	N=C-Ni-Cl (°)	86.49
Ni –N=C (imine) (Å)	2.171(5)	<Ar-N-Ni-N=C (°)	77.60 (5)
Ni-Cl (Å)	2.4167(14)	<Cl-Ni-OH_2 (°)	88.03 (5)
Ni-OH_2 (Å)	2.049(7)		

2. NMR analysis

^{1}H, ^{13}C{1H} and ^{19}F{1H} NMR spectra of the compounds

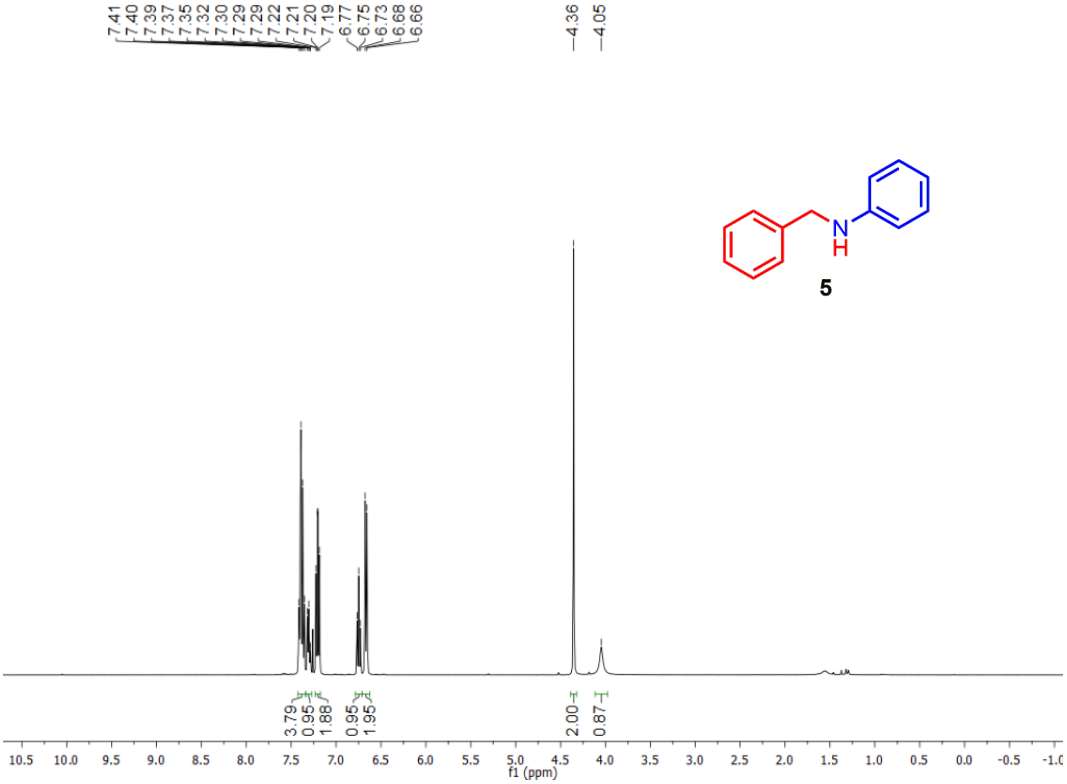

Figure S1. ^{1}H NMR spectra of *N*-benzylaniline (**5**)

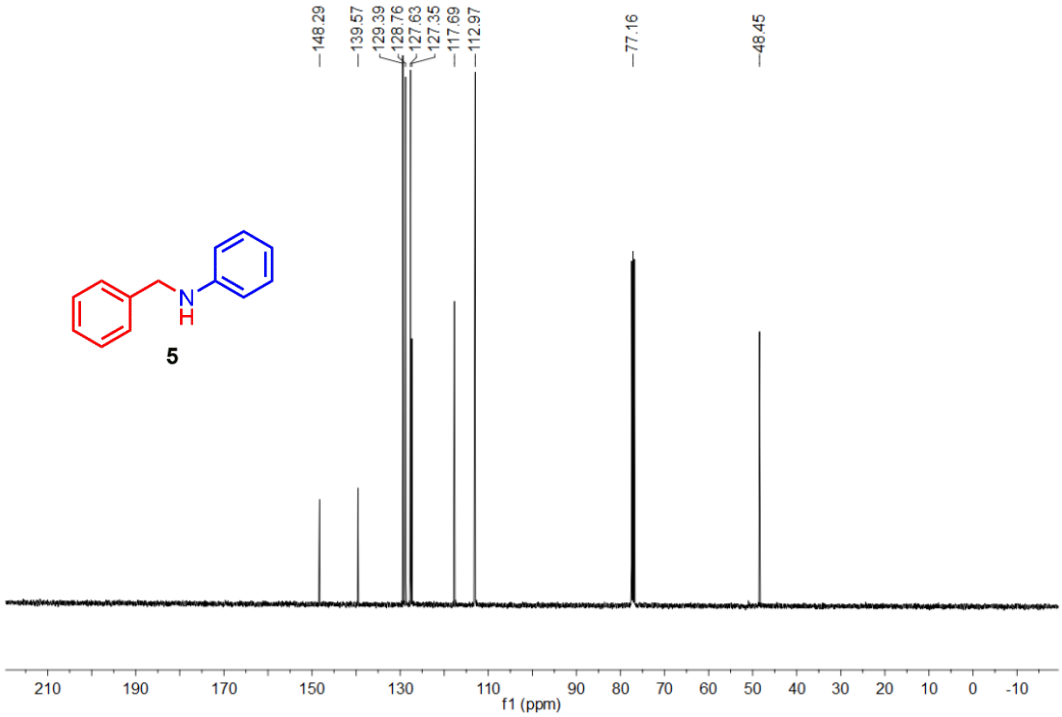

Figure S2. ^{13}C{1H} NMR spectra of *N*-benzylaniline (**5**)

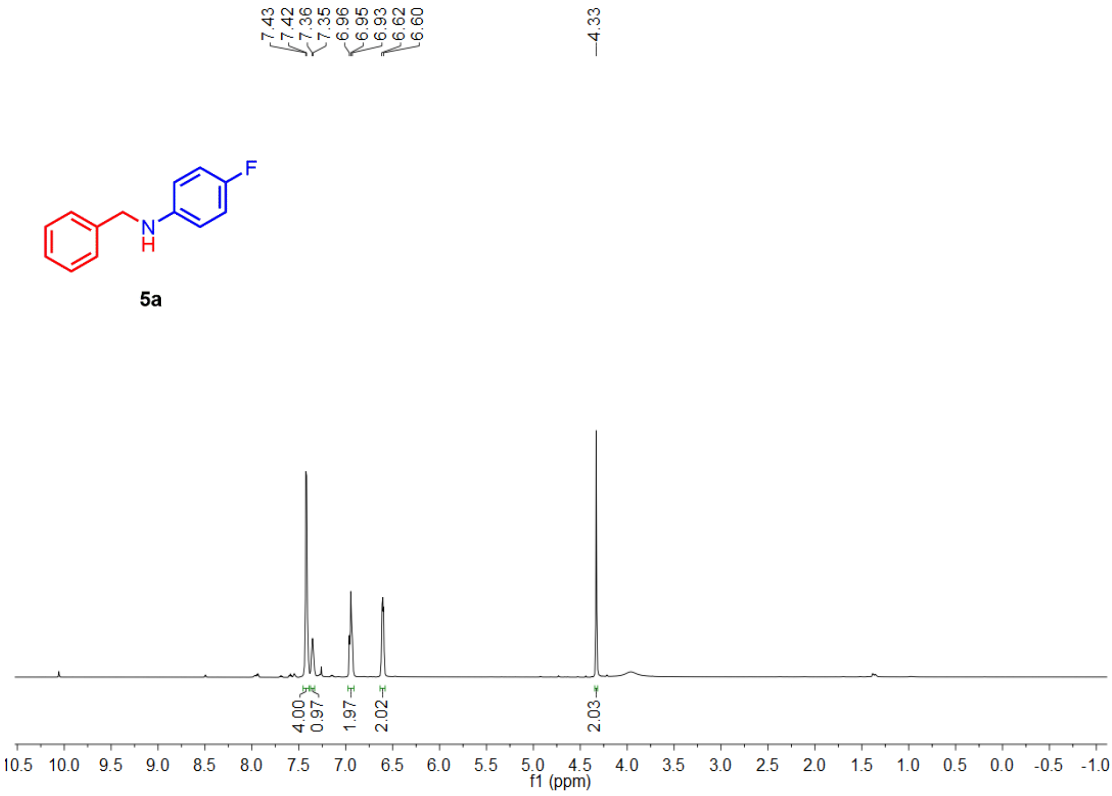

Figure S3. ^{1}H NMR spectra of *N*-benzyl-4-fluoroaniline (**5a**)

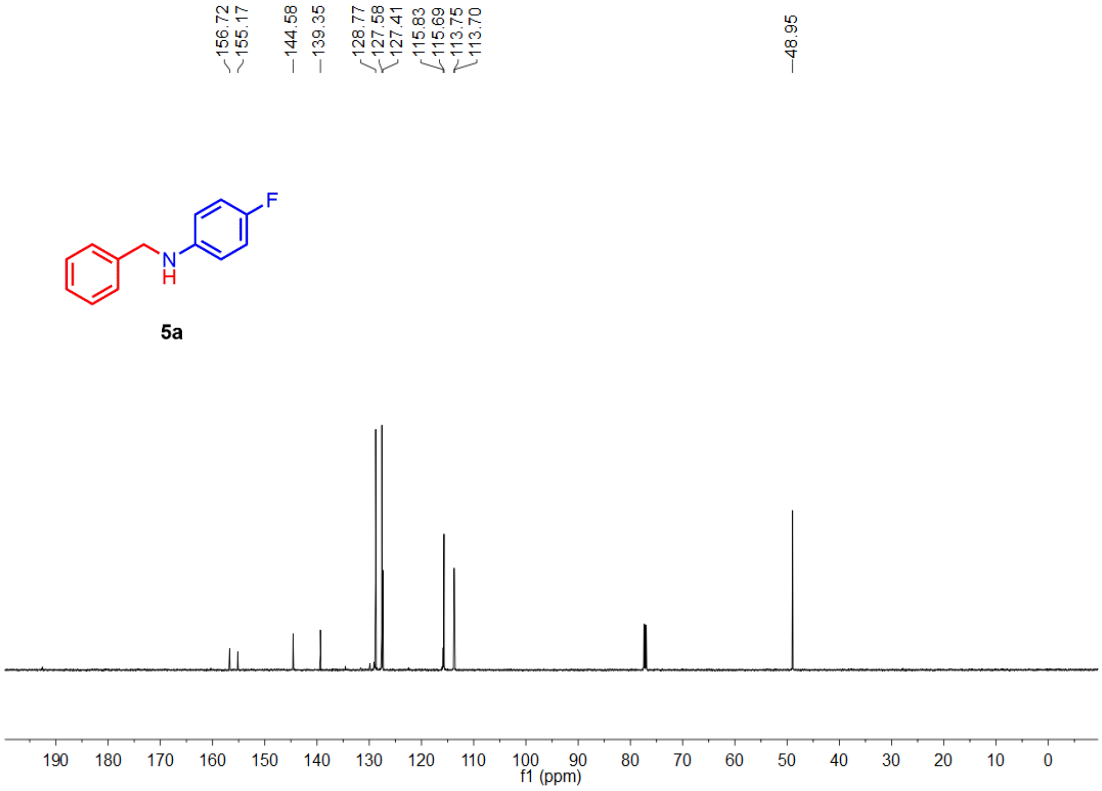

Figure S4. $^{13}C\{^{1}H\}$ NMR spectra of *N*-benzyl-4-fluoroaniline (**5a**)

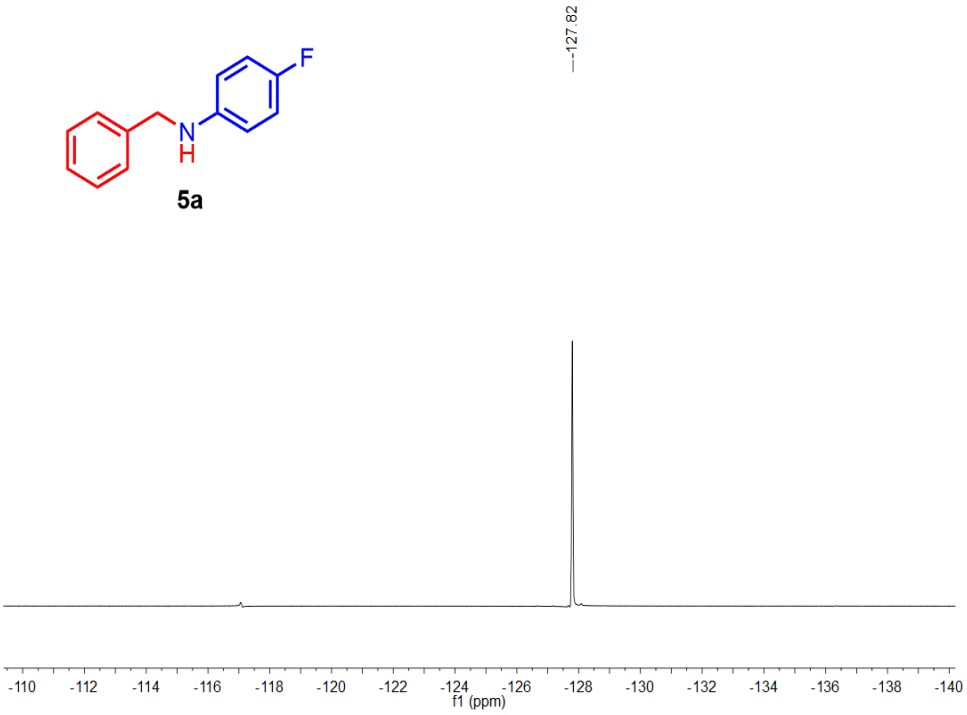

Figure S5. ^{19}F NMR spectra of *N*-benzyl-4-fluoroaniline (**5a**)

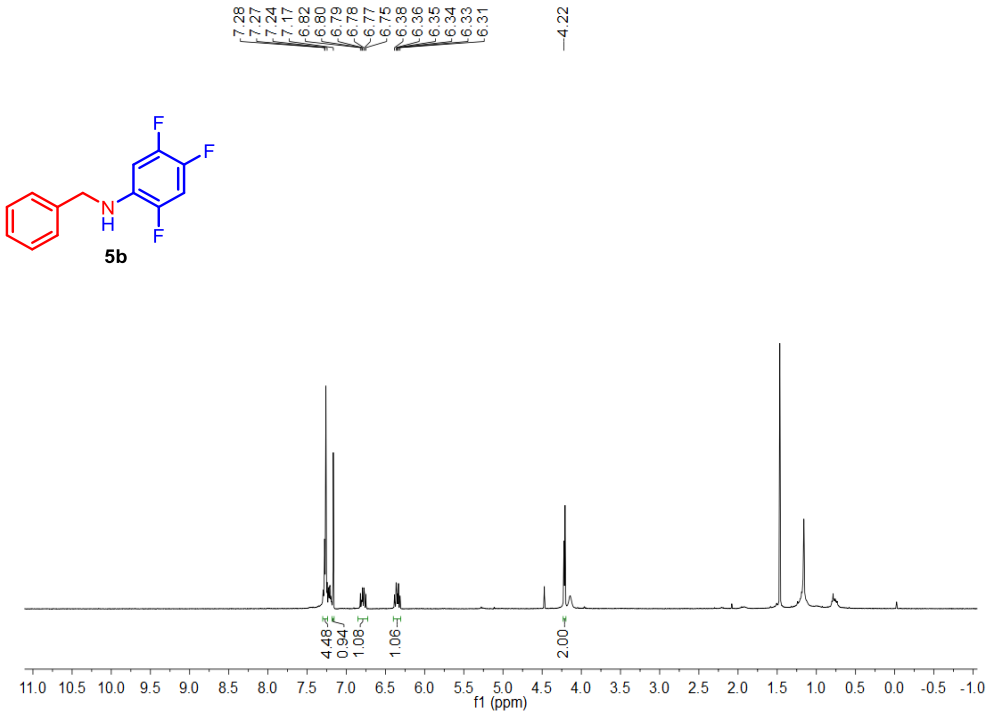

Figure S6. ^{1}H NMR spectra of *N*-benzyl-2,4,5-trifluoroaniline (**5b**)

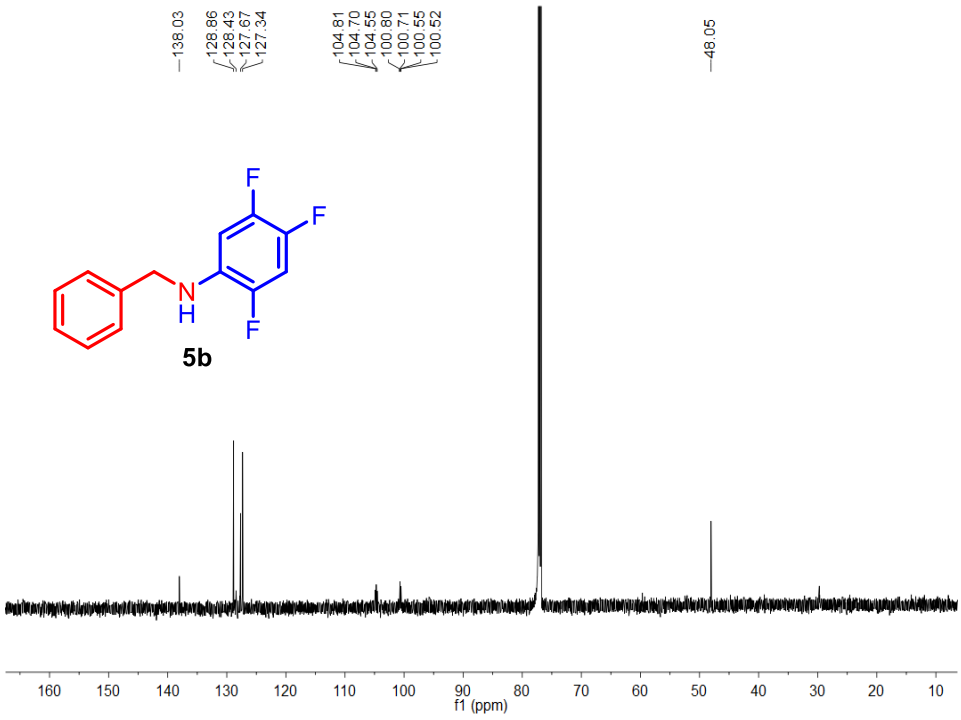

Figure S7. $^{13}C\{^{1}H\}$ NMR spectra of *N*-benzyl-2,4,5-trifluoroaniline (**5b**)

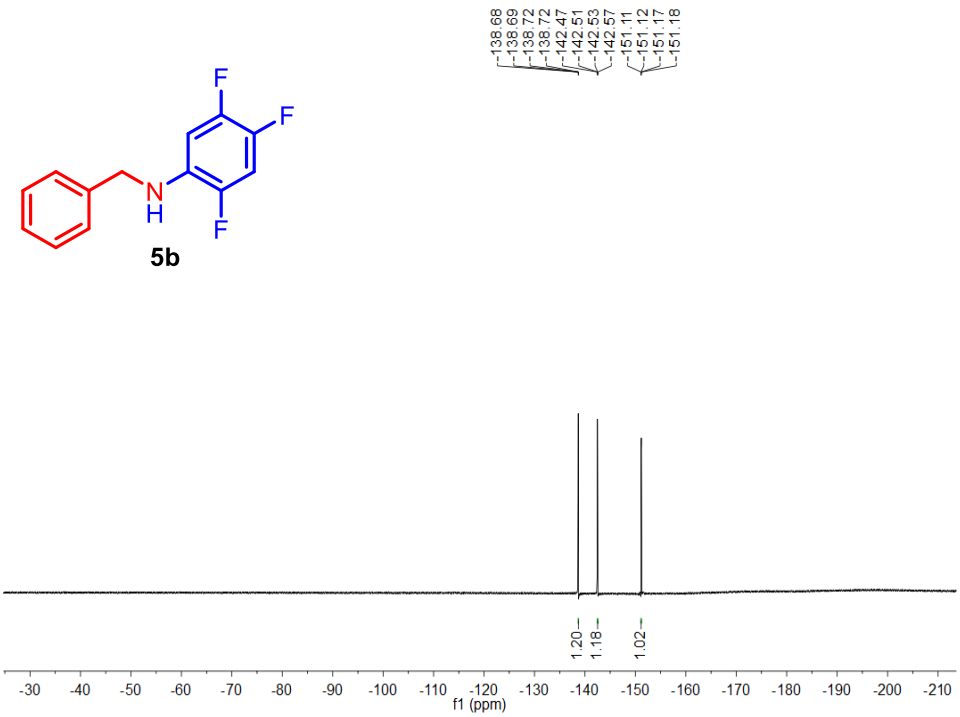

Figure S8. ^{19}F NMR spectra of *N*-benzyl-2,4,5-trifluoroaniline (**5b**)

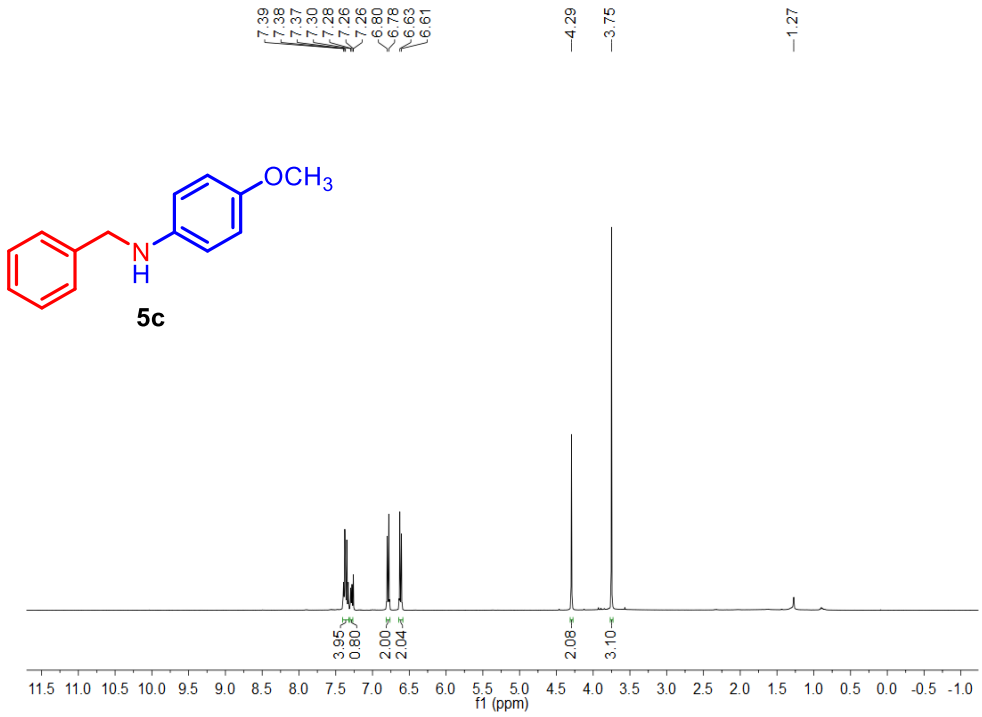

Figure S9. ^{1}H NMR spectra of *N*-benzyl-4-methoxyaniline (**5c**)

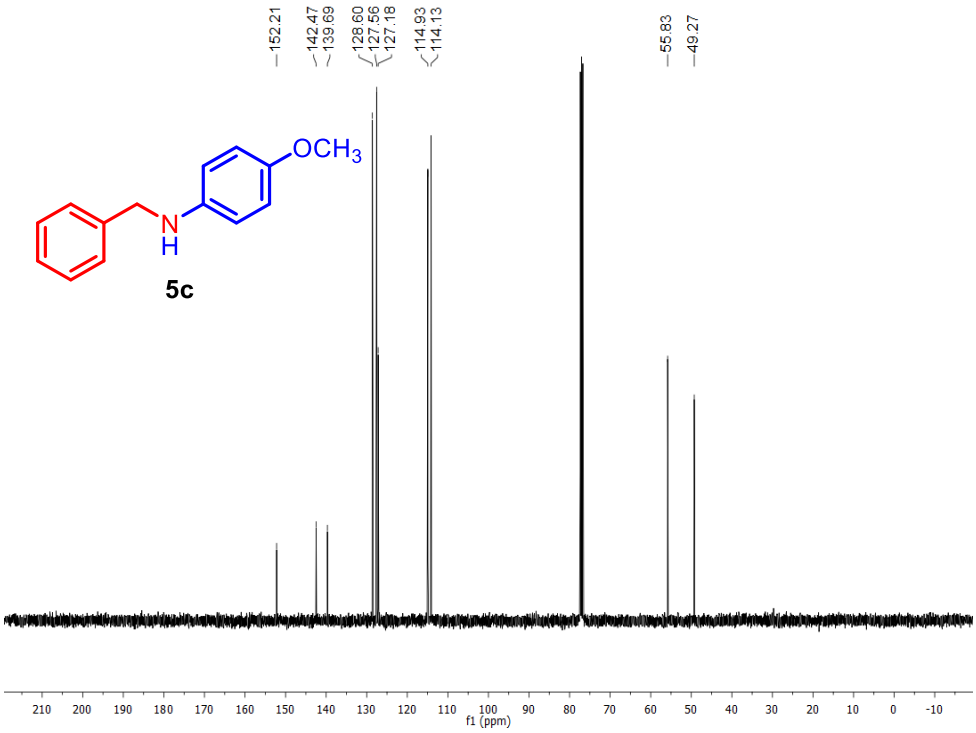

Figure S10. ^{13}C{1H} NMR spectra of *N*-benzyl-4-methoxyaniline (**5c**)

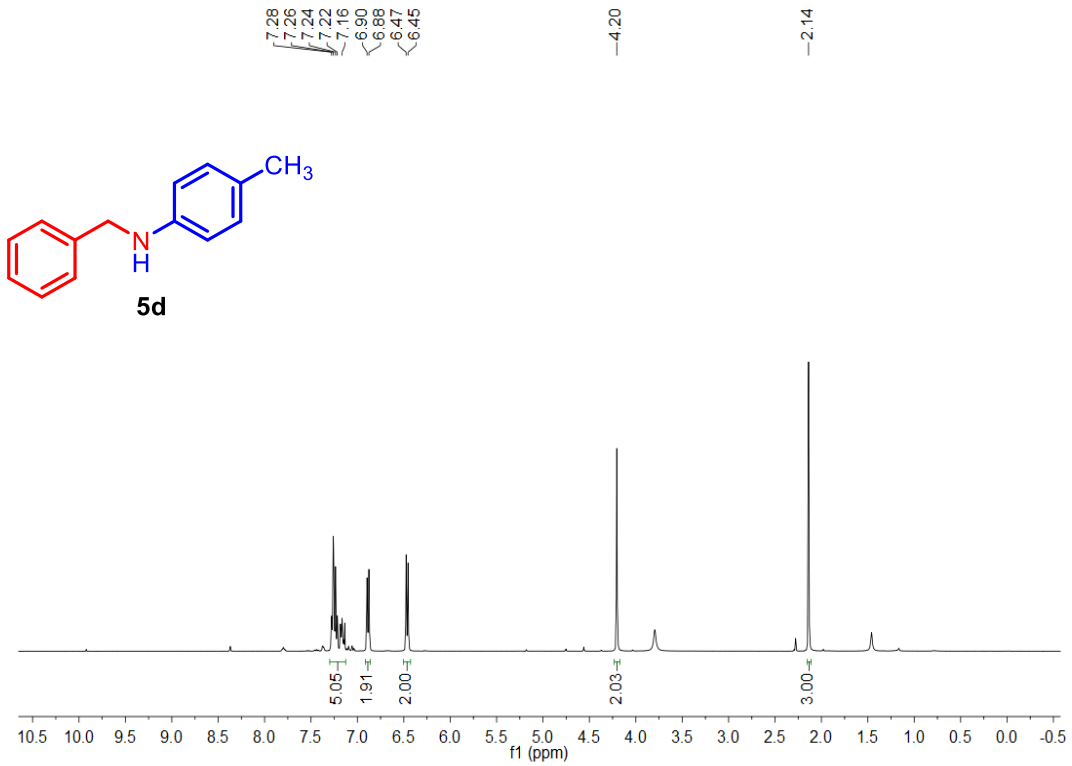

Figure S11. ^{1}H NMR spectra of *N*-benzyl-4-methylaniline (**5d**)

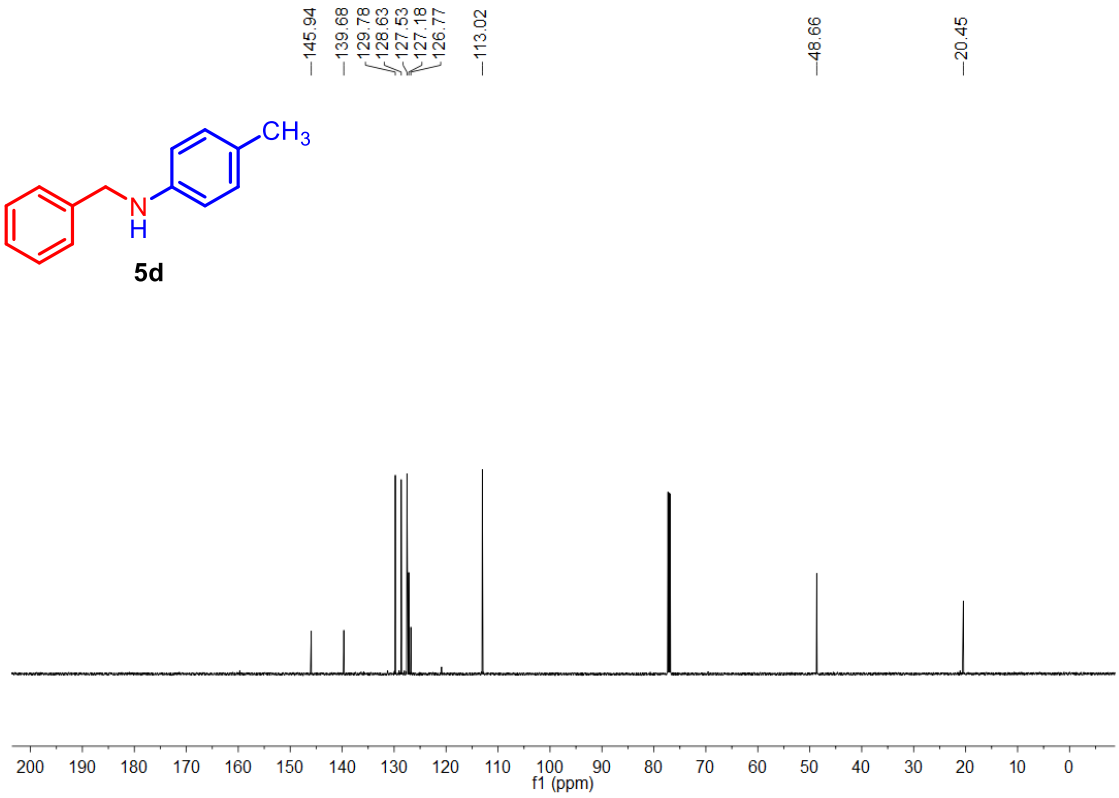

Figure S12. ^{13}C{^{1}H} NMR spectra of *N*-benzyl-4-methylaniline (**5d**)

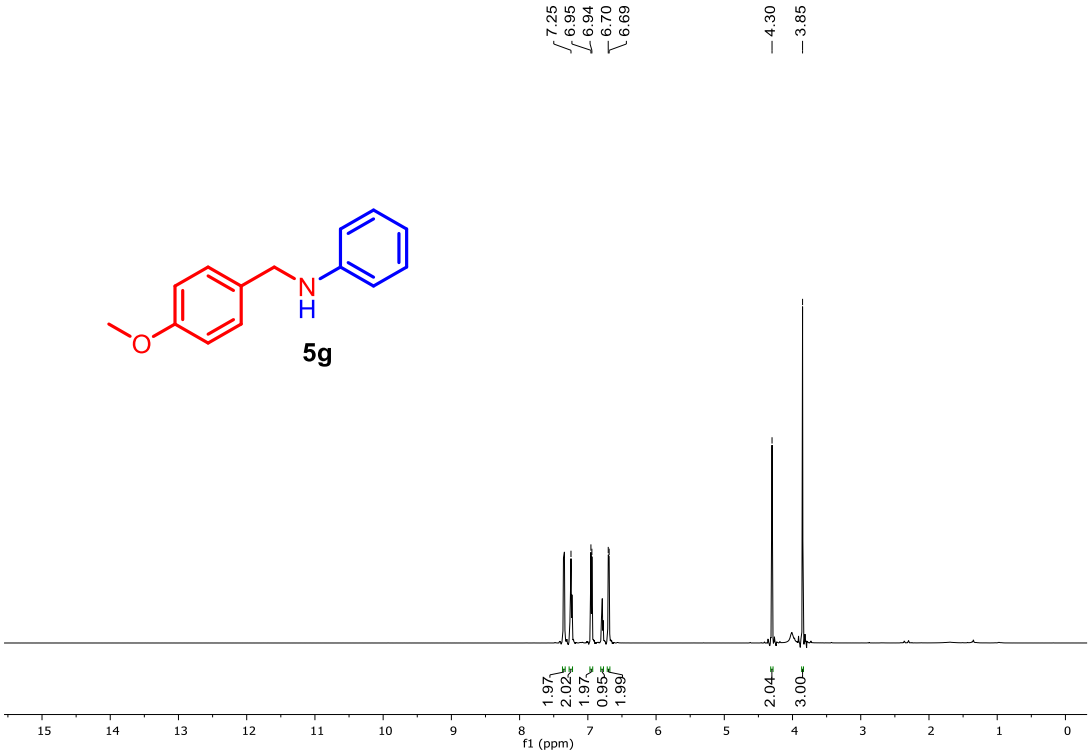

Figure S13. ^{1}H NMR spectra of *N*-(4-methoxybenzyl)aniline (**5g**)

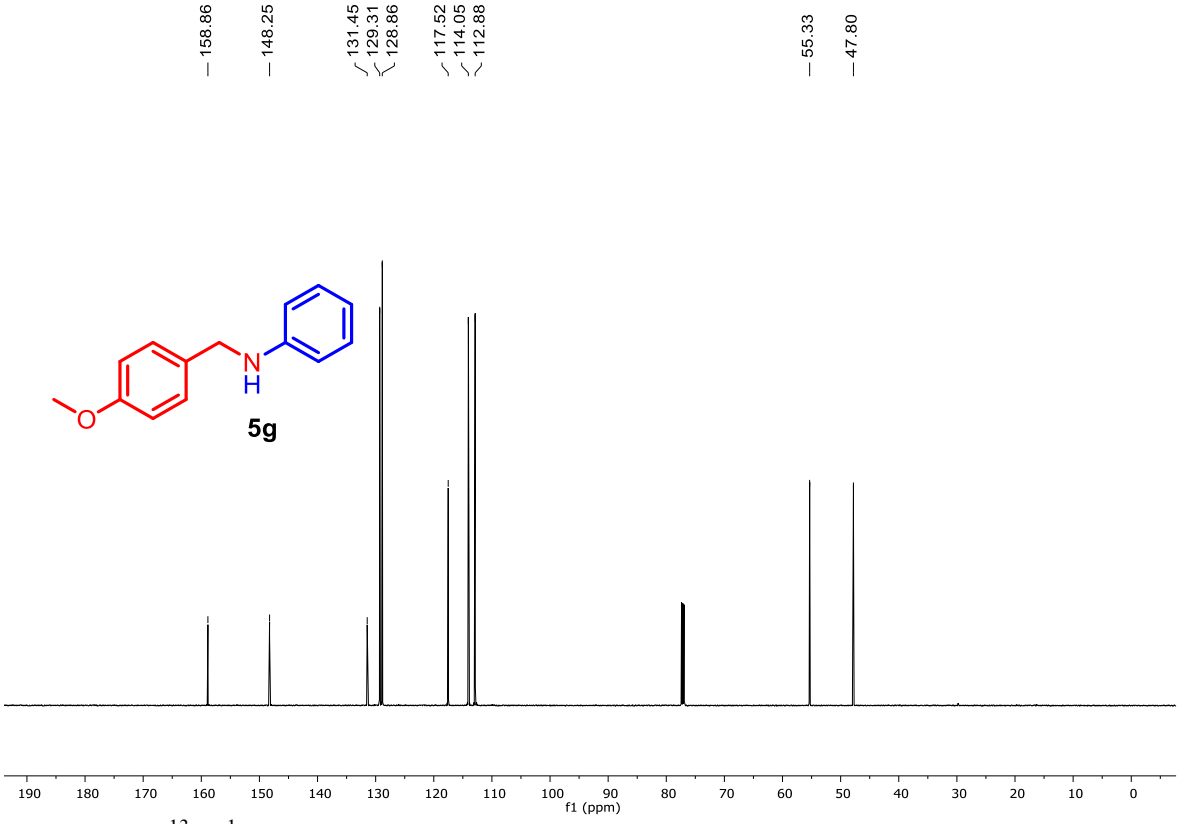

Figure S14. ^{13}C{^{1}H} NMR spectra of *N*-(4-methoxybenzyl)aniline (**5g**)

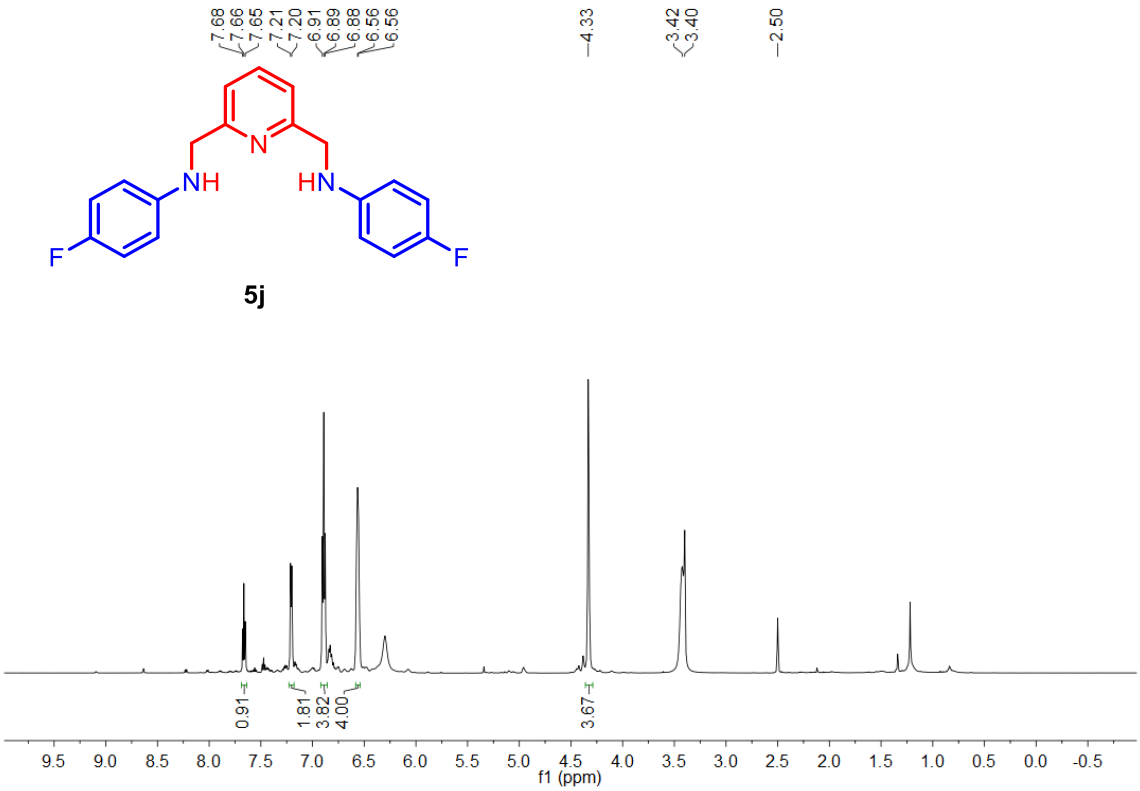

Figure S15. ^{1}H NMR spectra of *N,N′*-(pyridine-2,6-diylbis(methylene))bis(4-fluoroaniline)(**5j**)

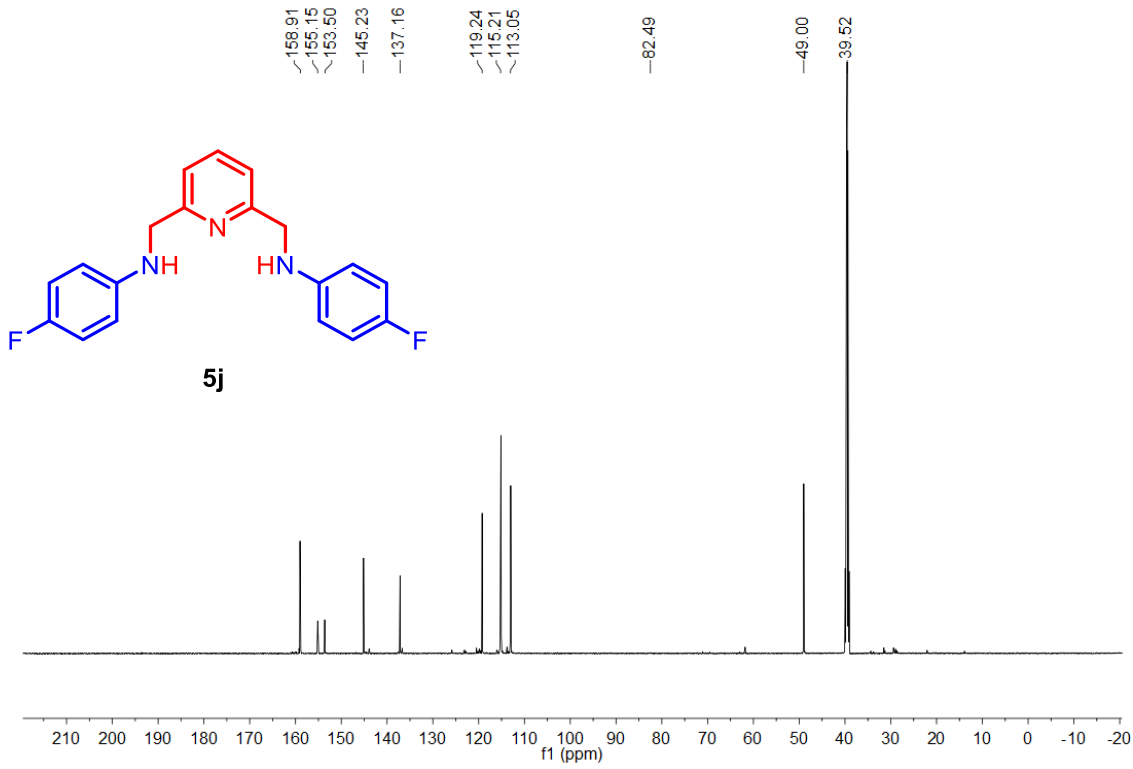

Figure S16. ^{13}C{^{1}H} NMR spectra of *N,N′*-(pyridine-2,6-diylbis(methylene))bis(4-fluoroaniline) (**5j**)

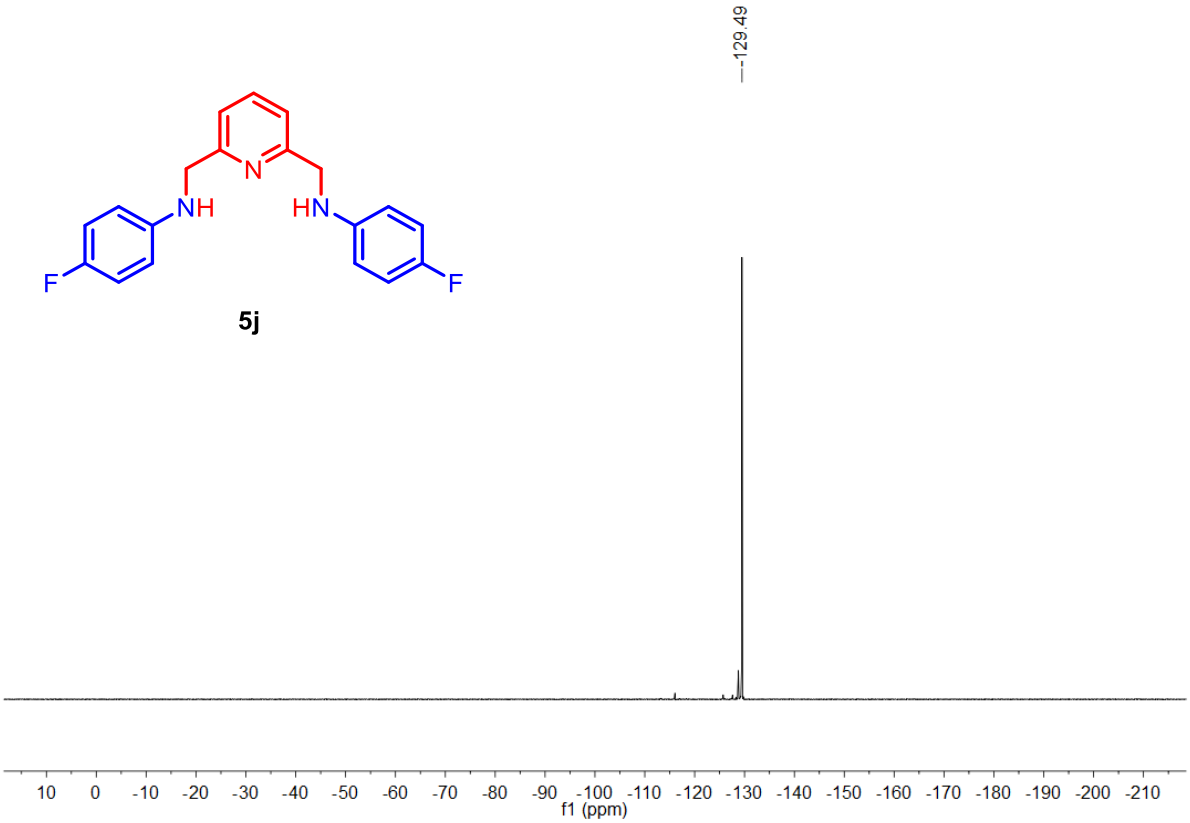

Figure S17. ^{19}F NMR spectra of *N,N′*-(pyridine-2,6-diylbis(methylene))bis(4-fluoroaniline) (**5j**)

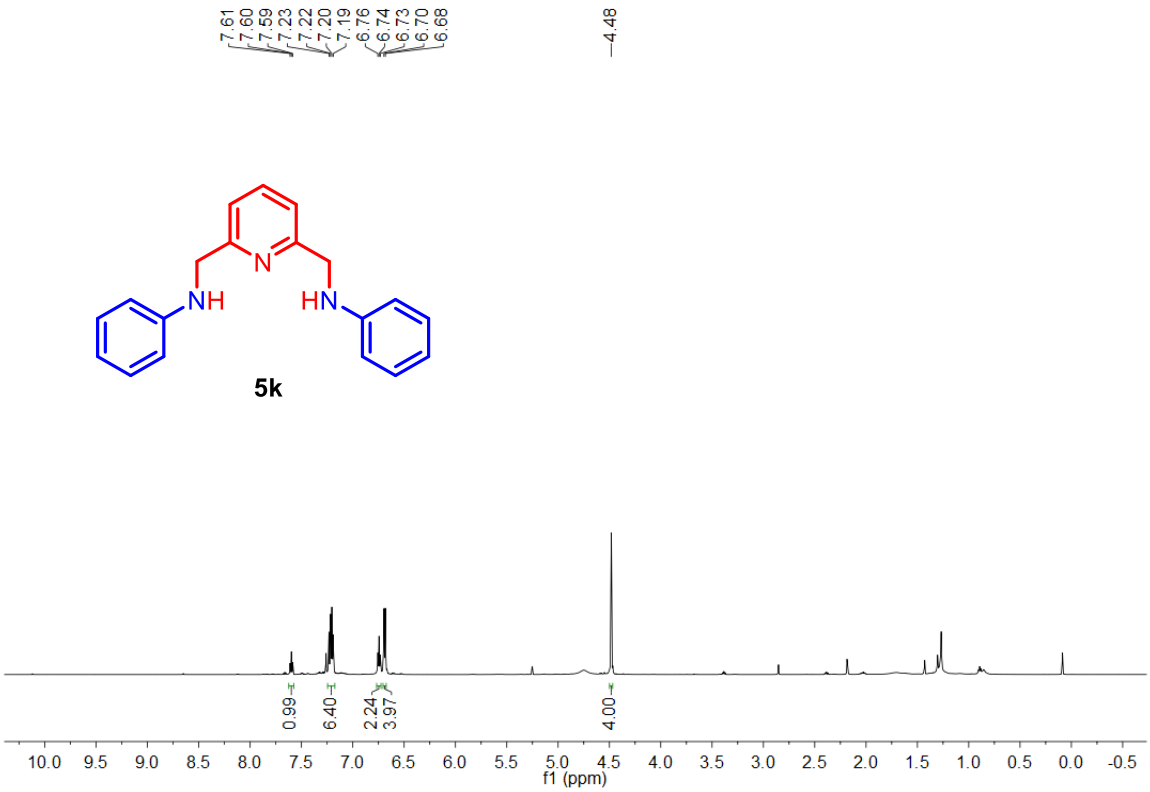

Figure S18. ^{1}H NMR spectra of *N,N′*-(pyridine-2,6-diylbis(methylene))dianiline (**5k**)

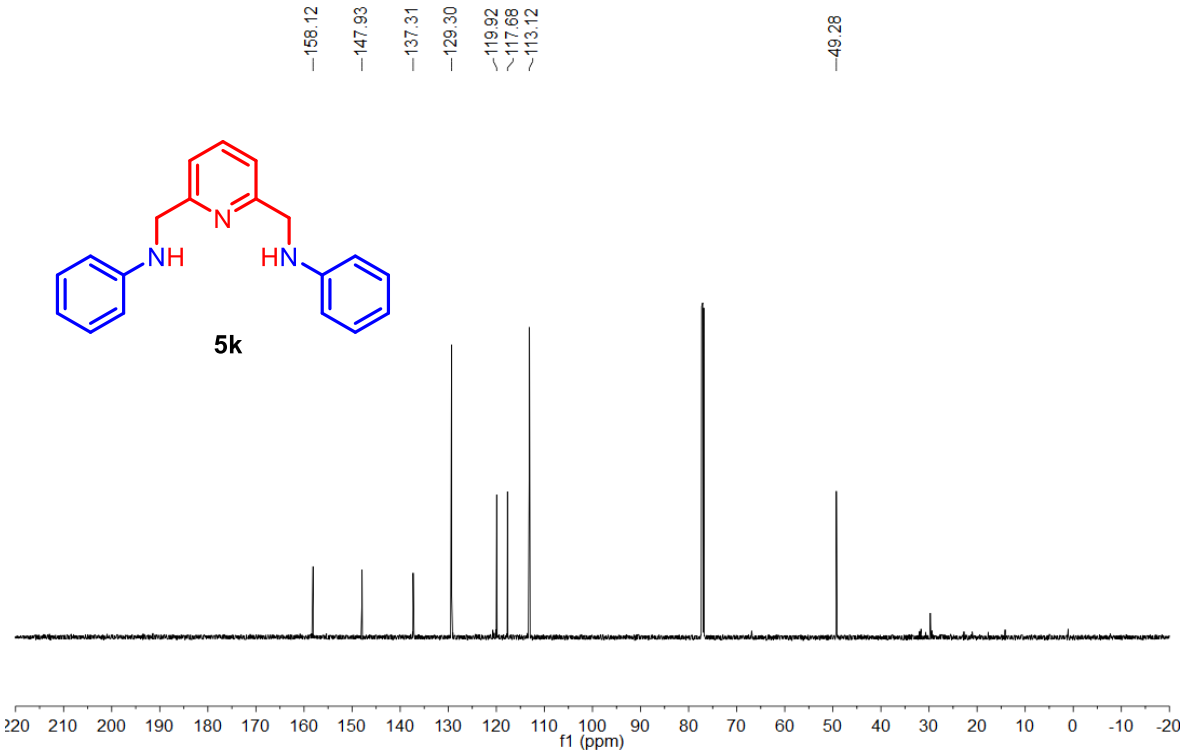

Figure S19. 13C{^{1}H} NMR spectra of *N,N′*-(pyridine-2,6-diylbis(methylene))dianiline (**5k**)

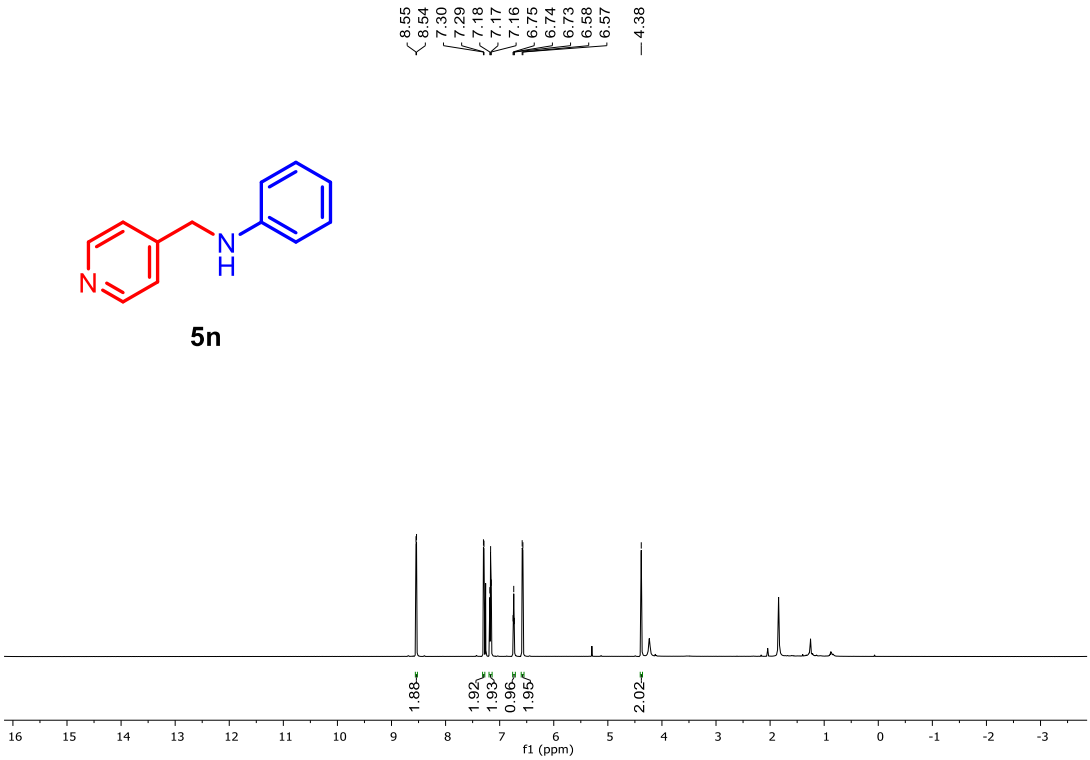

Figure S20. ^{1}H NMR spectra of *N*-(pyridin-4-ylmethyl)aniline (**5n)**

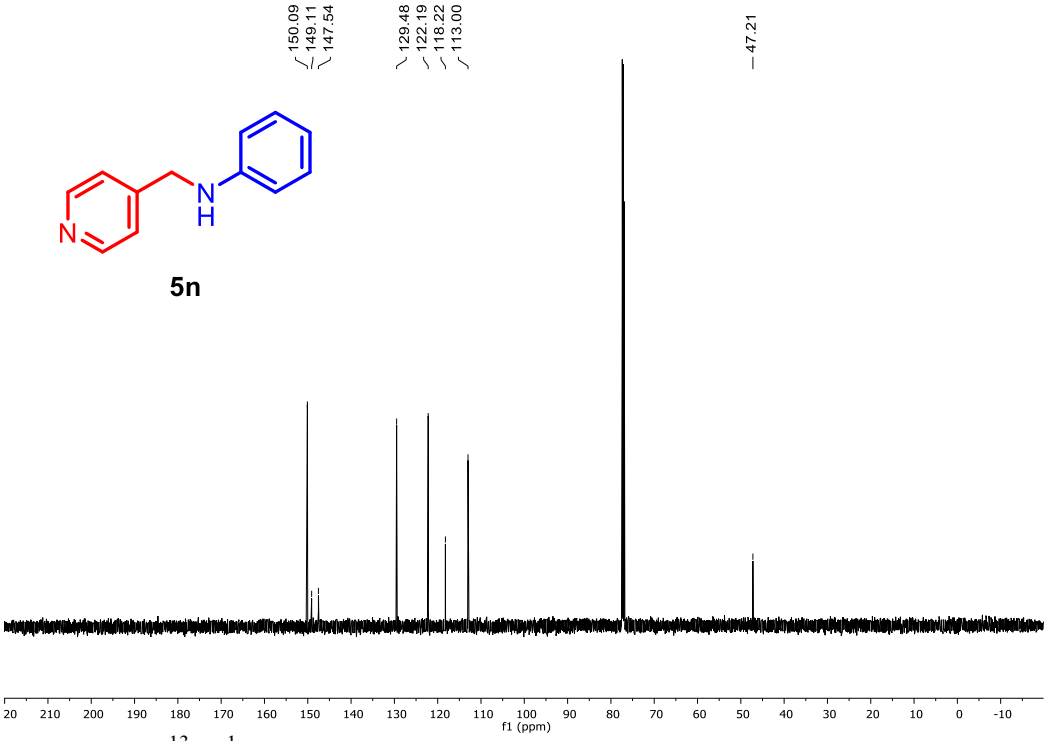

Figure S21. $^{13}C\{^{1}H\}$ NMR spectra of *N*-(pyridin-4-ylmethyl)aniline (**5n**)

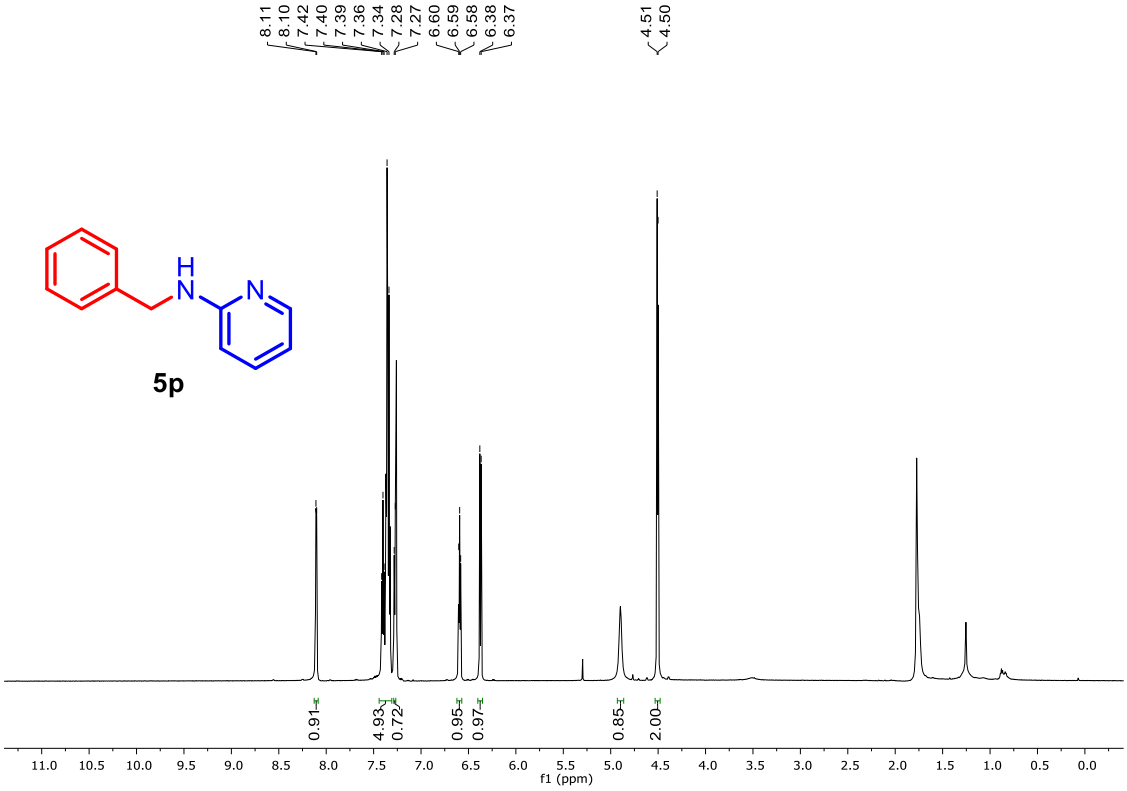

Figure S22. ^{1}H NMR spectra of N-benzylpyridin-2-amine (**5p**)

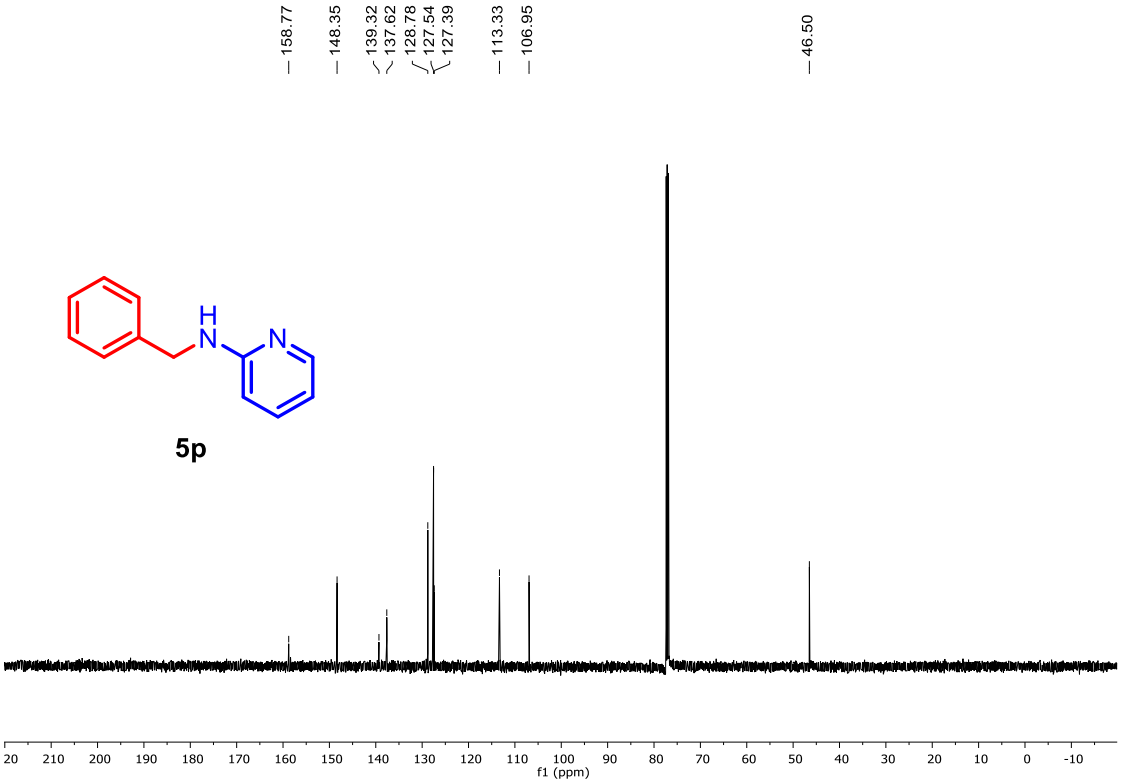

Figure S23. 13C{^{1}H} NMR spectra of N-benzylpyridin-2-amine (**5p**)

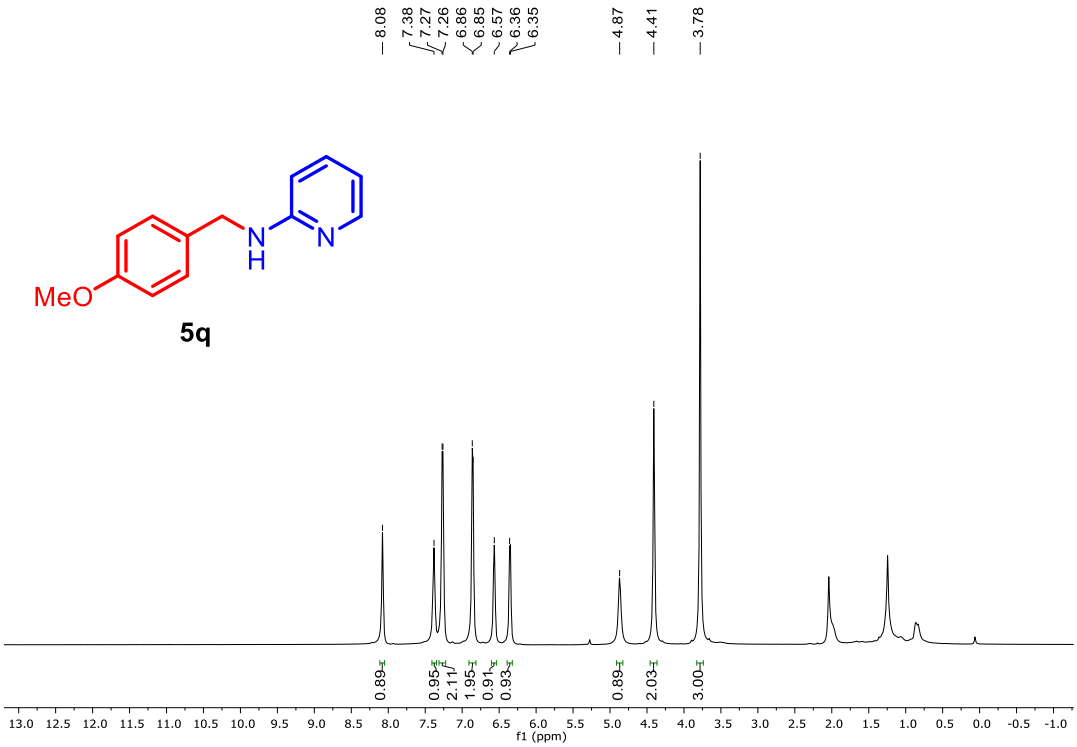

Figure S24. ^{1}H NMR spectra of *N*-(4-methoxybenzyl)pyridin-2-amine (**5q**)

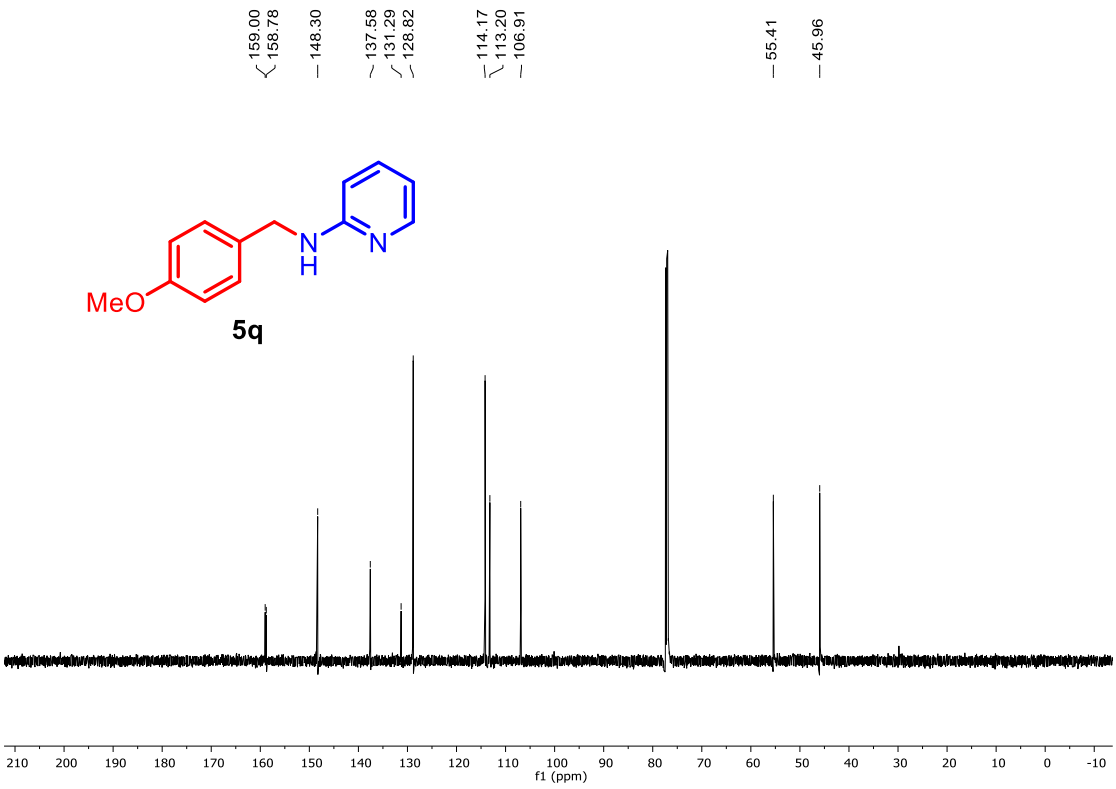

Figure S25. $^{13}C\{^{1}H\}$ NMR spectra of *N*-(4-methoxybenzyl)pyridin-2-amine (**5q**)

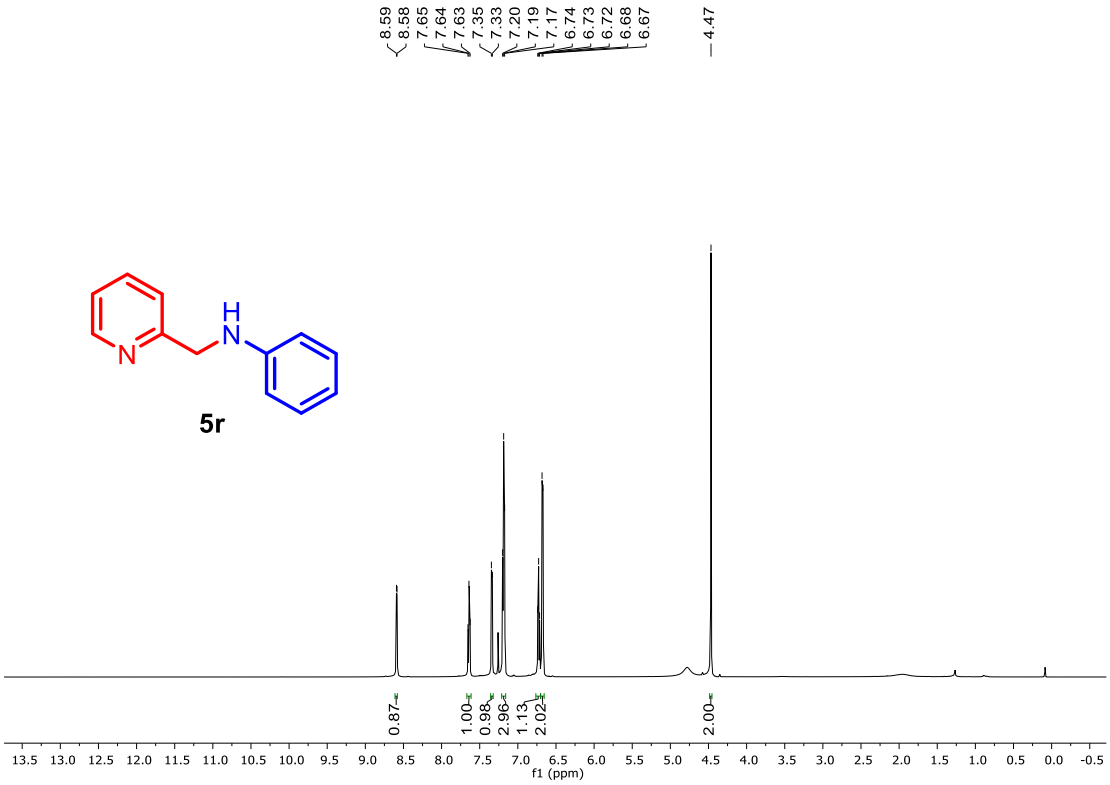

Figure S26. ^{1}H NMR spectra of N-(pyridin-2-ylmethyl)aniline (**5r**)

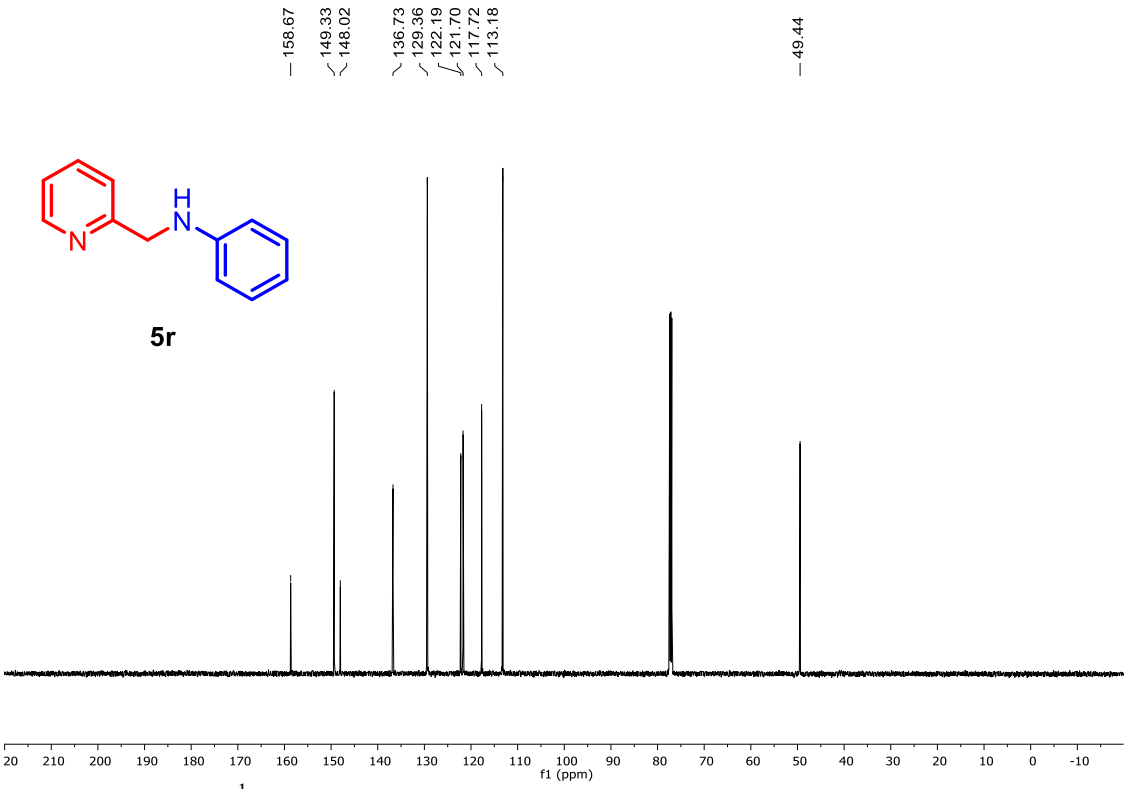

Figure S27. 13C{^{1}H} NMR spectra of N-(pyridin-2-ylmethyl)aniline (**5r**)

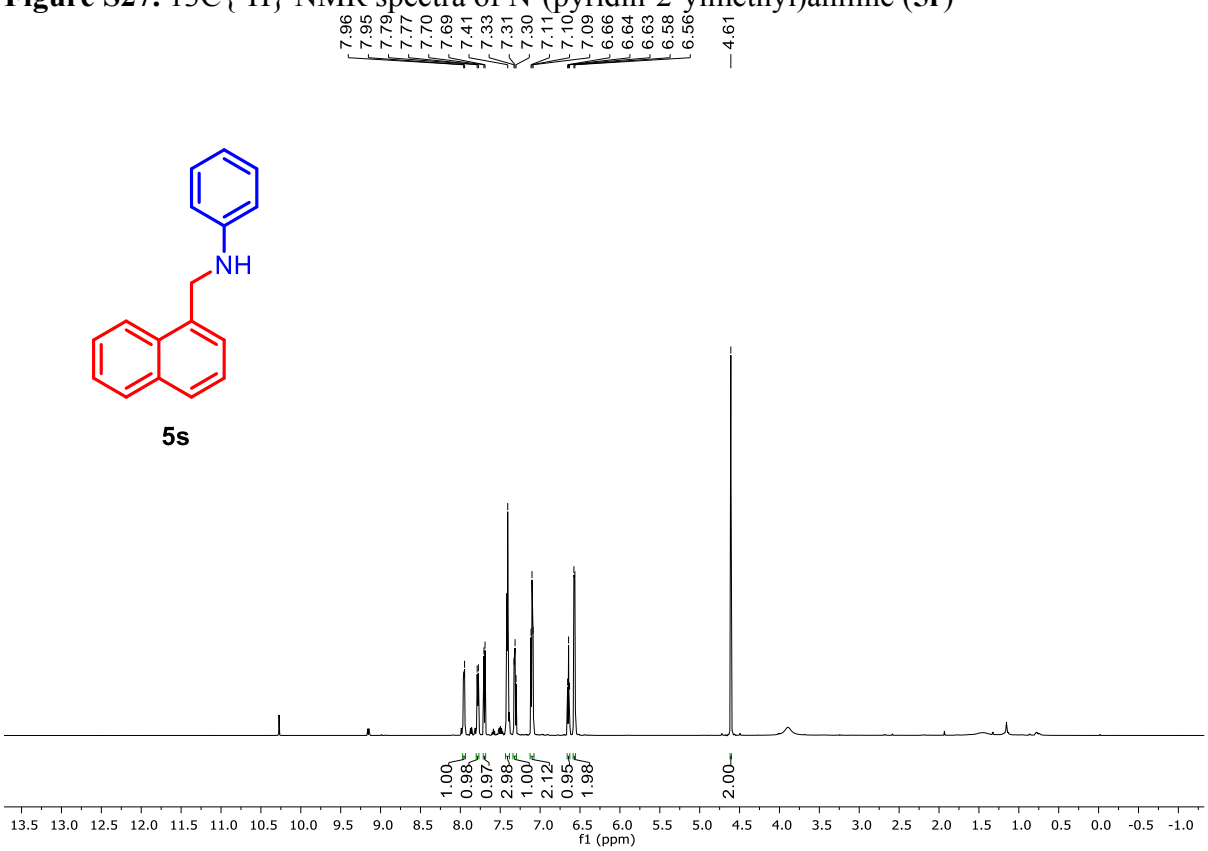

Figure S28. ^{1}H NMR spectra of *N*-(naphthalen-1-ylmethyl)aniline (**5s**)

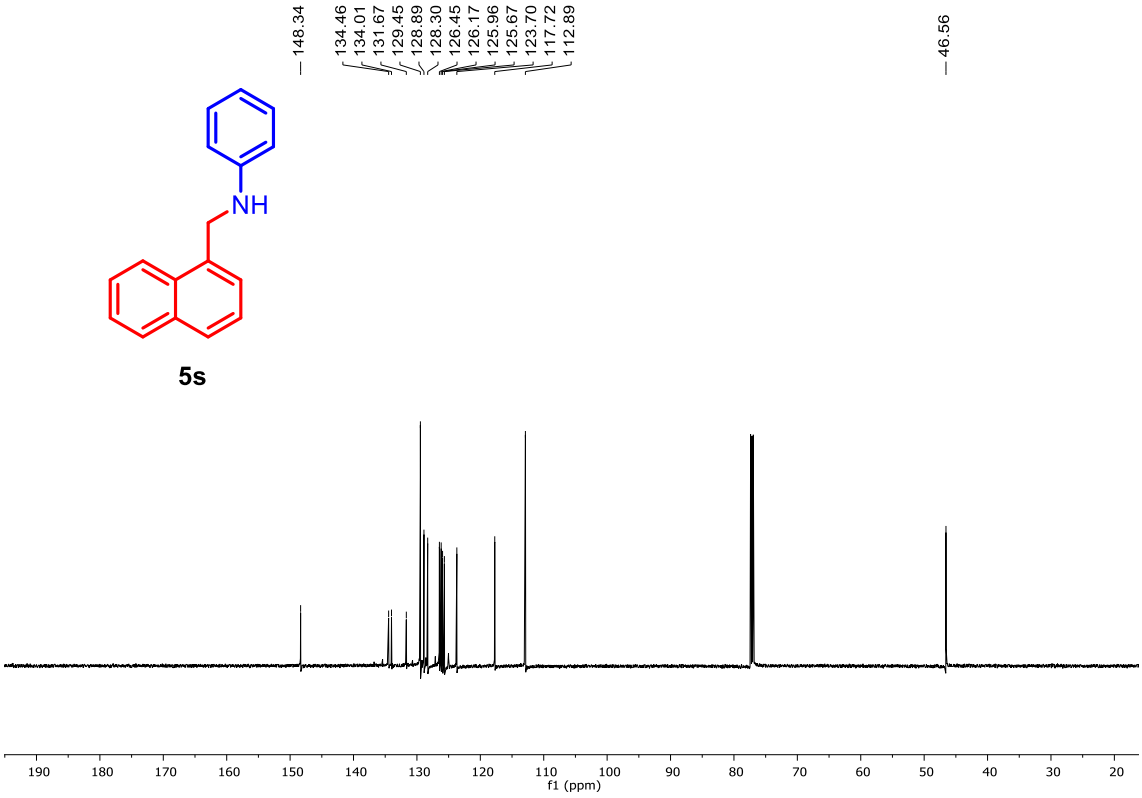

Figure S29. $^{13}C\{^{1}H\}$ NMR spectra of *N*-(naphthalen-1-ylmethyl)aniline (**5s**)

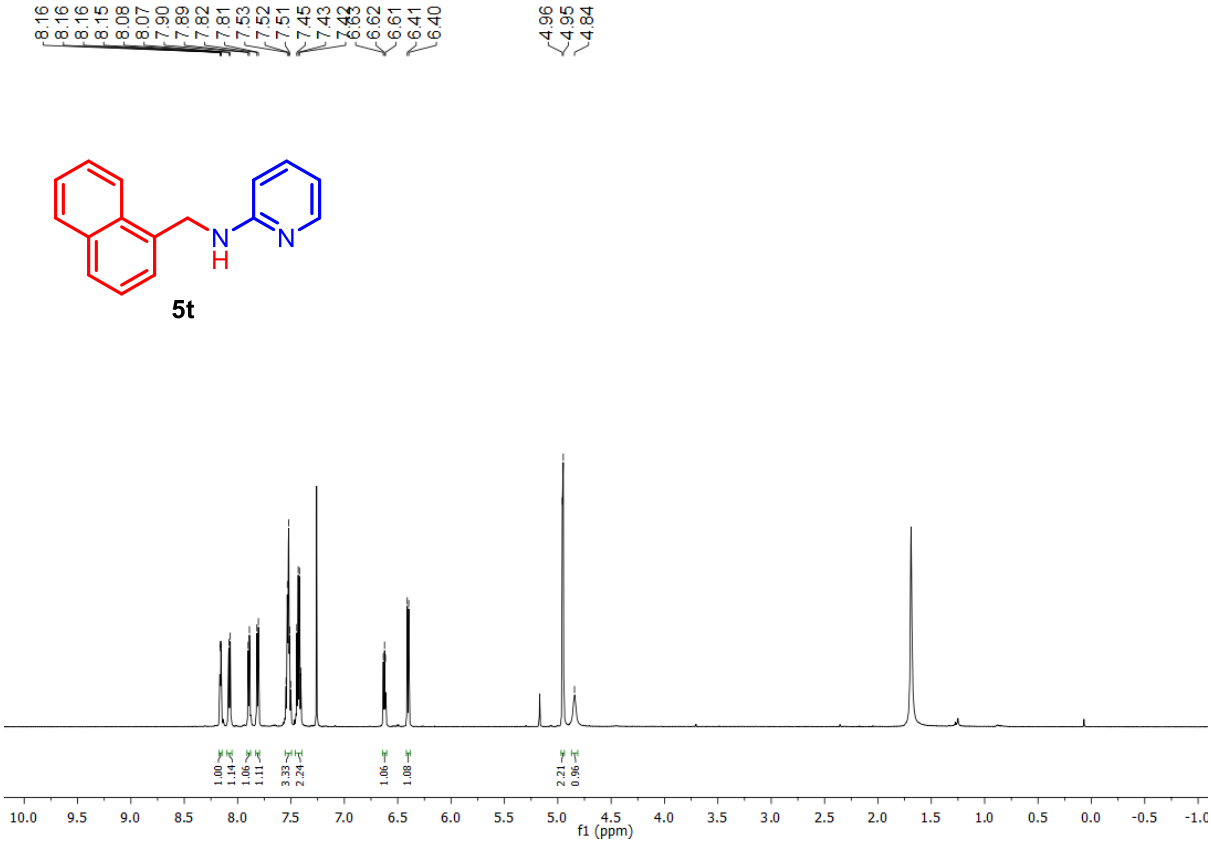

Figure S30. ^{1}H NMR spectra of *N*-(naphthalen-1-ylmethyl)pyridin-2-amine (**5t**)

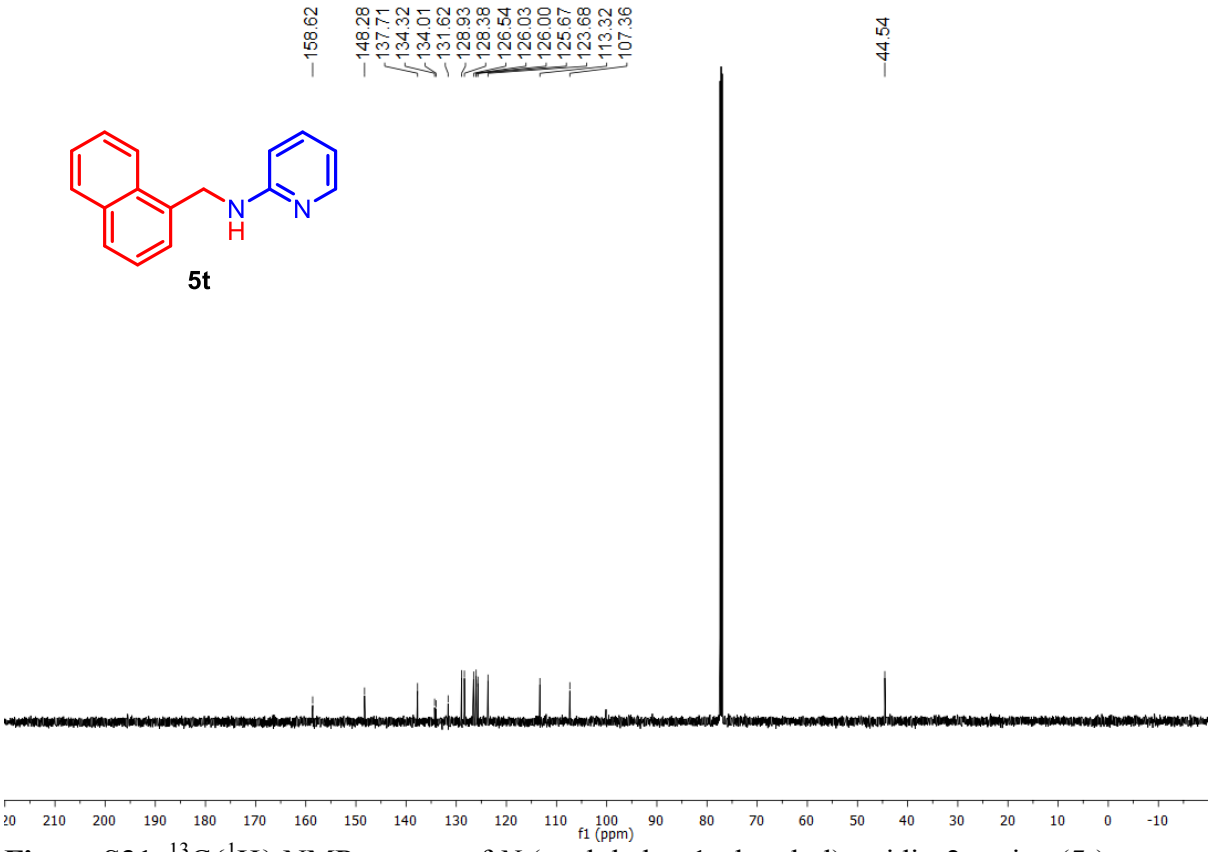

Figure S31. $^{13}C\{^{1}H\}$ NMR spectra of *N*-(naphthalen-1-ylmethyl)pyridin-2-amine (**5t**)

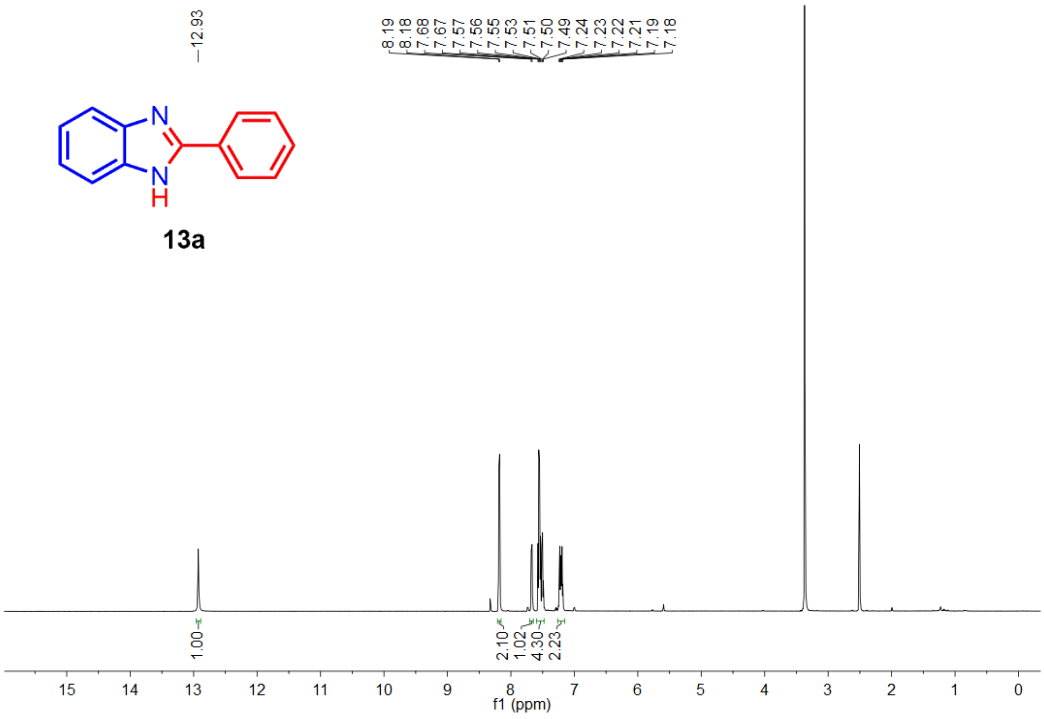

Figure S32. ^{1}H NMR spectra of 2-phenyl-1H-benzo[d]imidazole (**13a**)

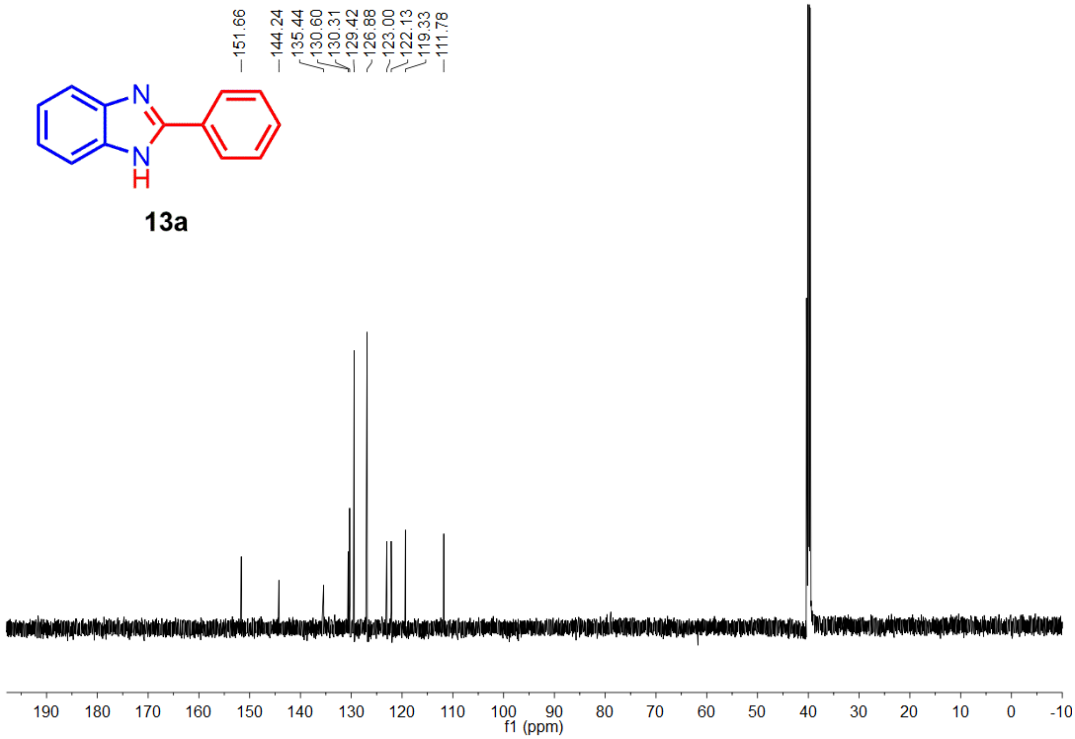

Figure S33. $^{13}C\{^{1}H\}$NMR spectra of 2-phenyl-1H-benzo[d]imidazole (**13a**)

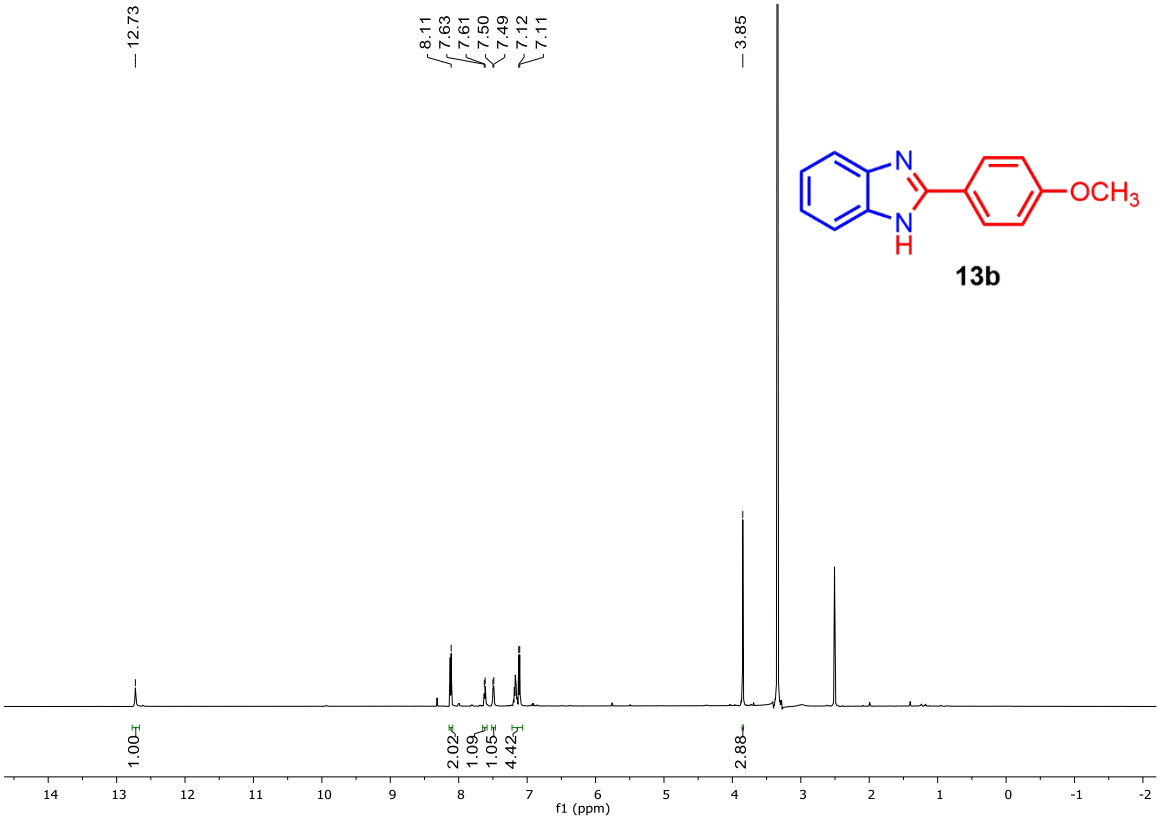

Figure S34. ^{1}H NMR spectra of 2-(4-methoxyphenyl)-1H-benzo[d]imidazole (**13b**)

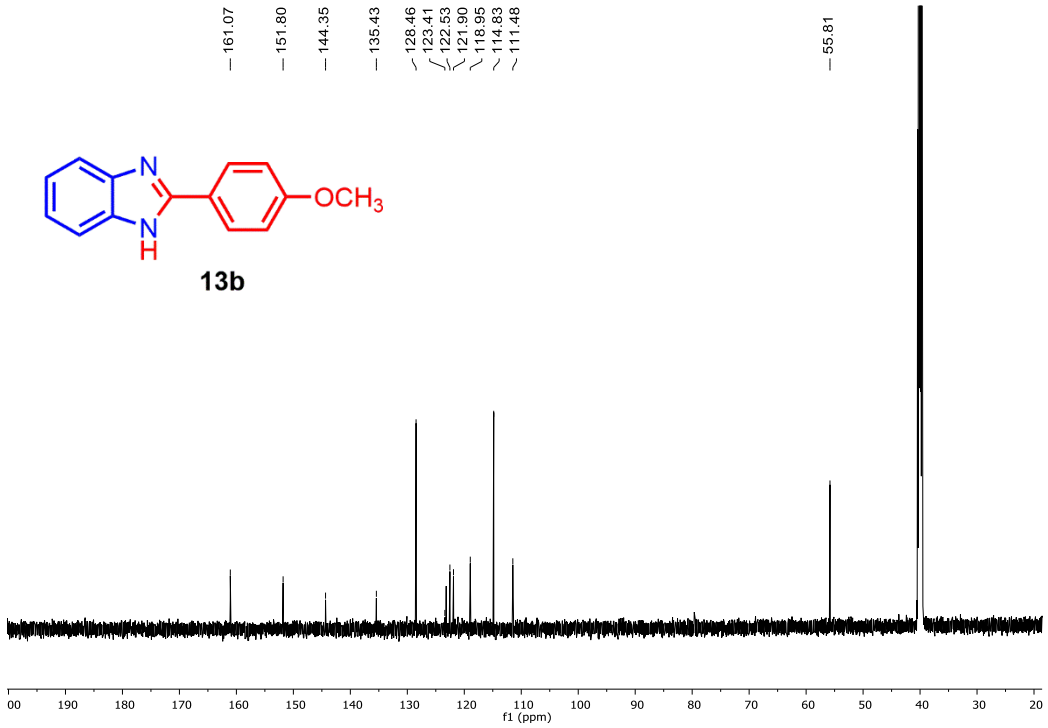

Figure S35. $^{13}C\{^{1}H\}$ NMR spectra of 2-(4-methoxyphenyl)-1H-benzo[d]imidazole (**13b**)

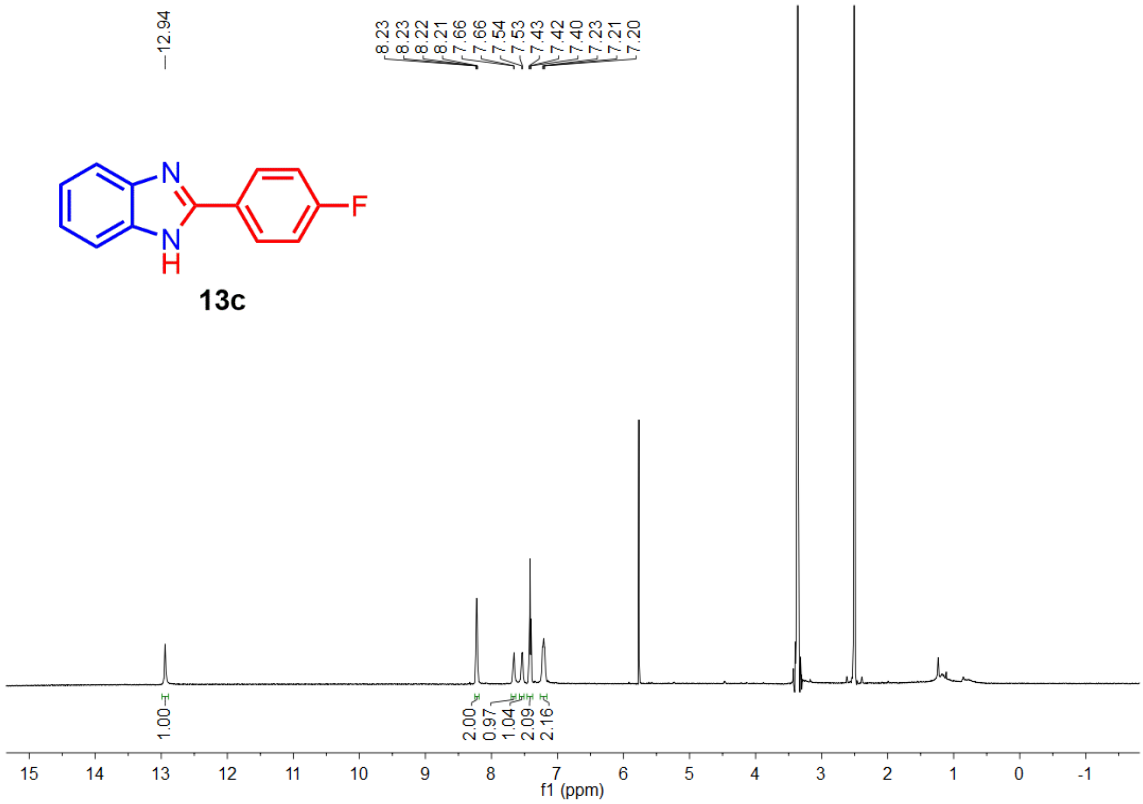

Figure S36. ^{1}H NMR spectra of 2-(4-fluorophenyl)-1H-benzo[d]imidazole (**13c**)

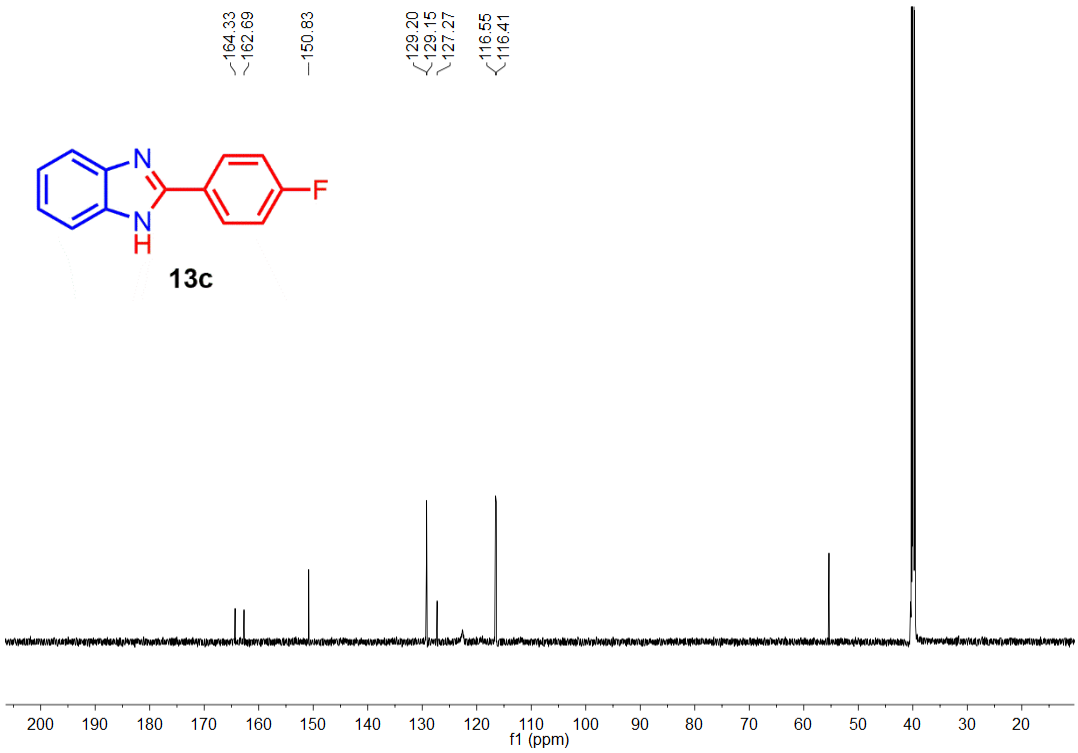

Figure S37. $^{13}C\{^{1}H\}$ NMR spectra of 2-(4-fluorophenyl)-1H-benzo[d]imidazole (**13c**)

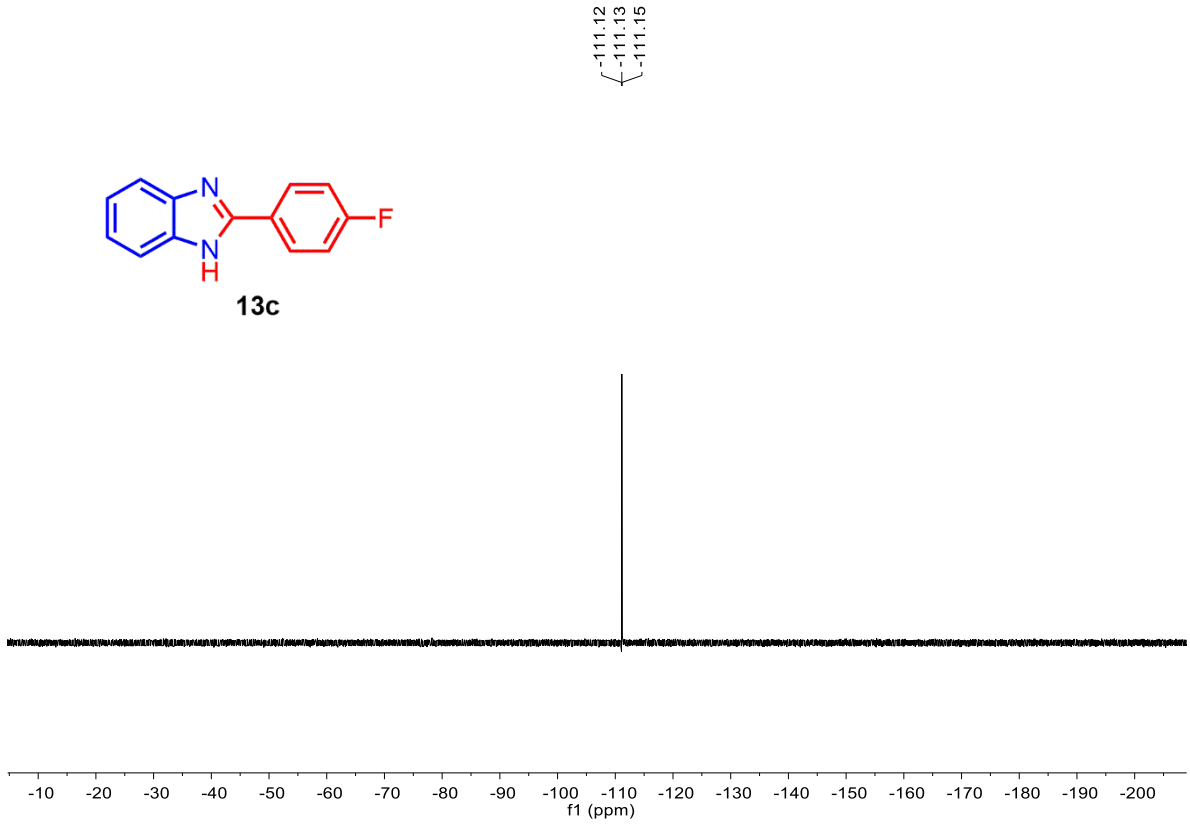

Figure S38. ^{19}F NMR spectra of 2-(4-fluorophenyl)-1H-benzo[d]imidazole (**13c**)

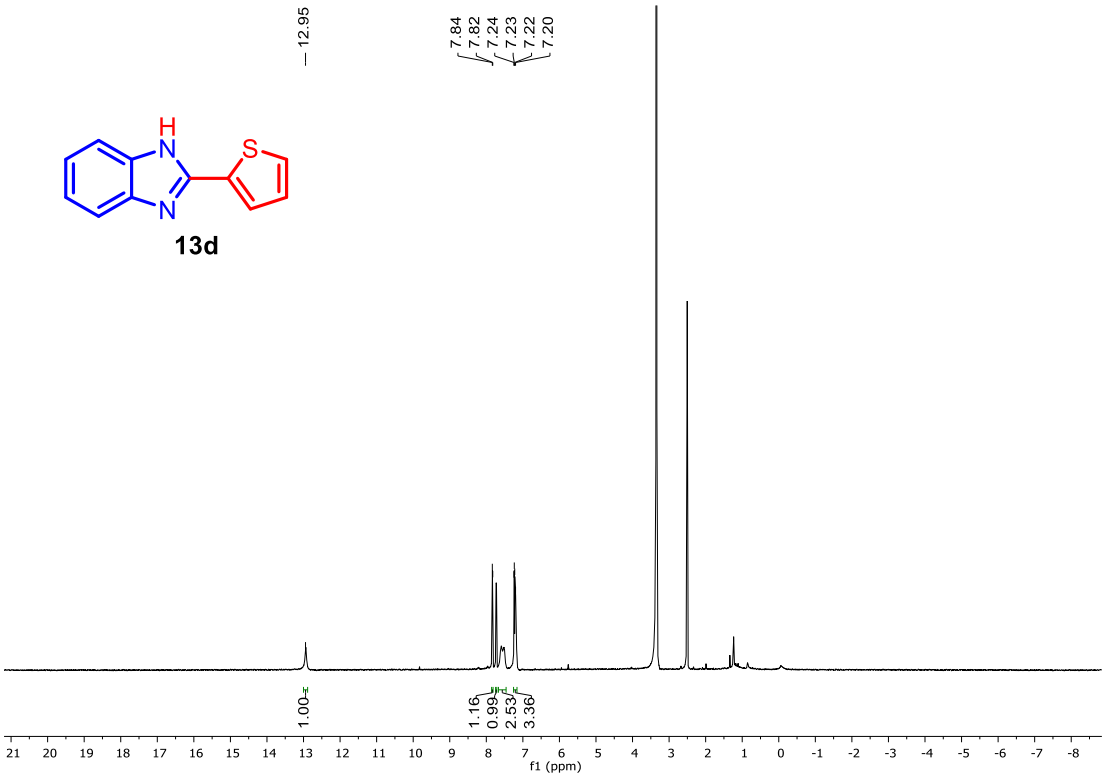

Figure S39. ^{1}H NMR spectra of 2-(thiophen-2-yl)-1H-benzo[d]imidazole (**13d**)

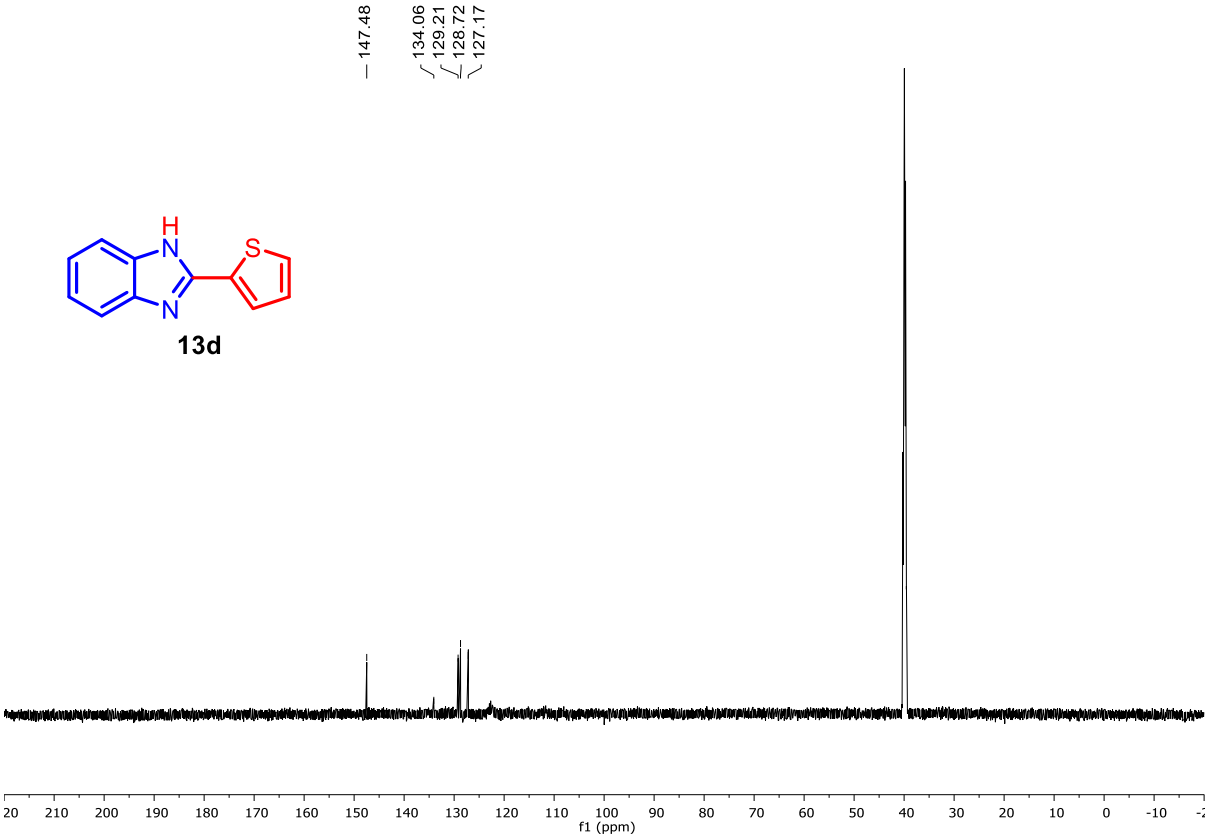

Figure S40. ^{13}C{^{1}H} NMR spectra of 2-(thiophen-2-yl)-1H-benzo[d]imidazole (**13d**)

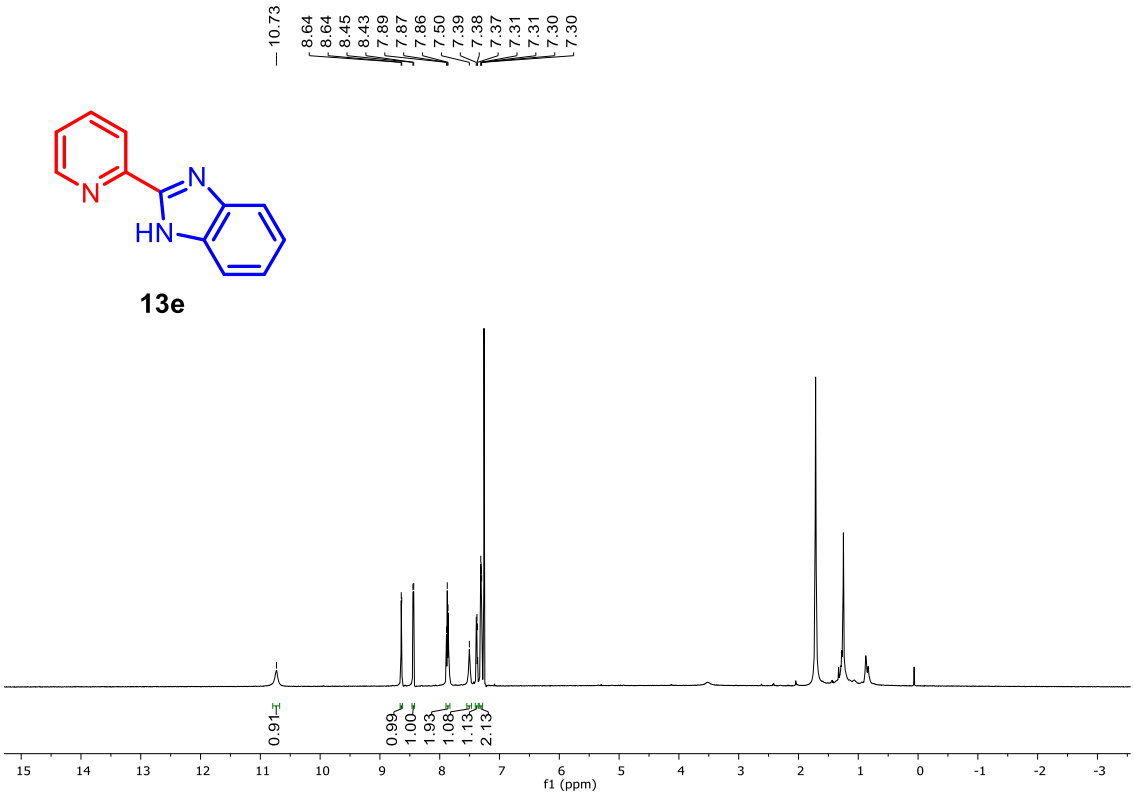

Figure S41. ^{1}H NMR spectra of 2-(pyridin-2-yl)-1H-benzo[d]imidazole (**13e**)

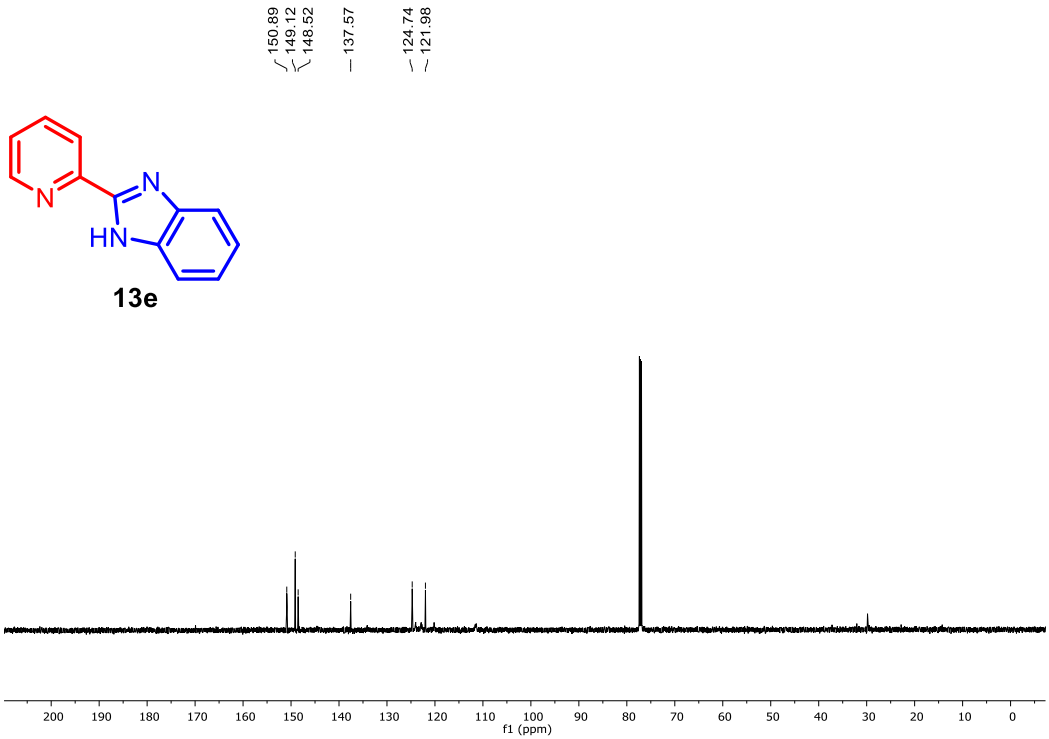

Figure S42. ^{13}C{^{1}H} NMR spectra of 2-(pyridin-2-yl)-1H-benzo[d]imidazole (**13e**)

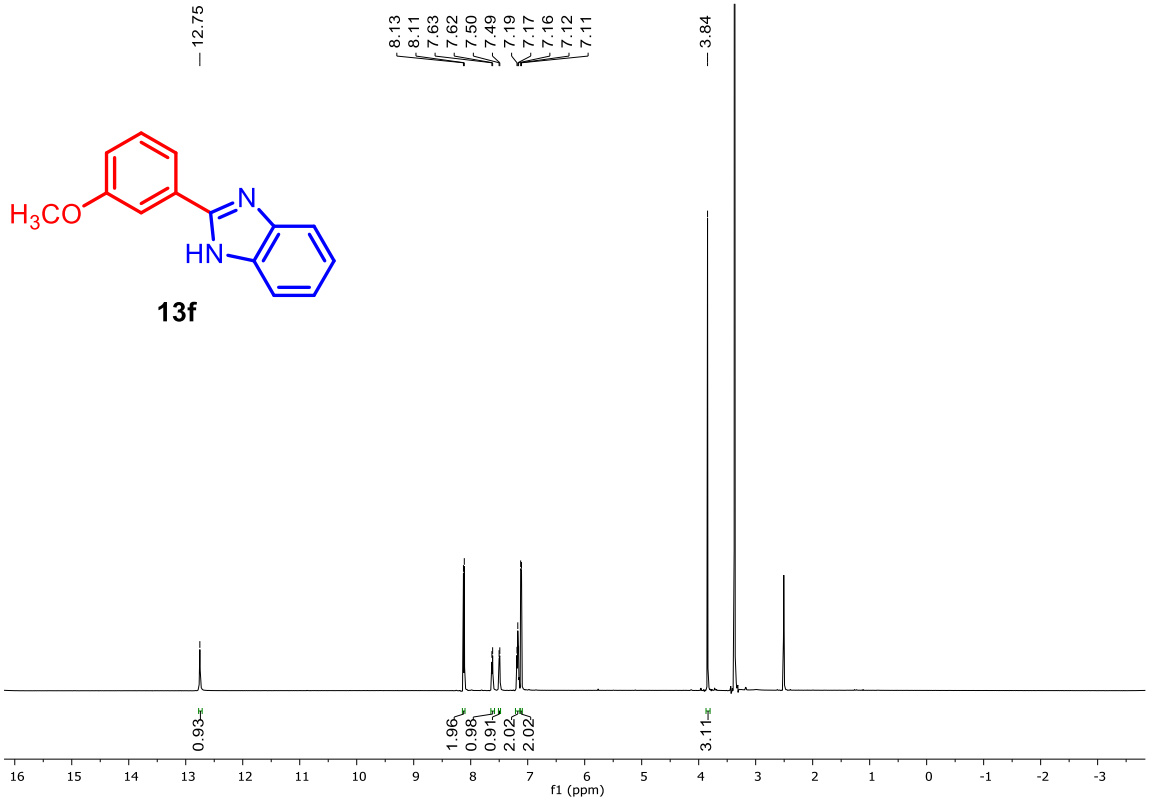

Figure S43. ^{1}H NMR spectra of 2-(3-methoxyphenyl)-1H-benzo[d]imidazole (**13f**)

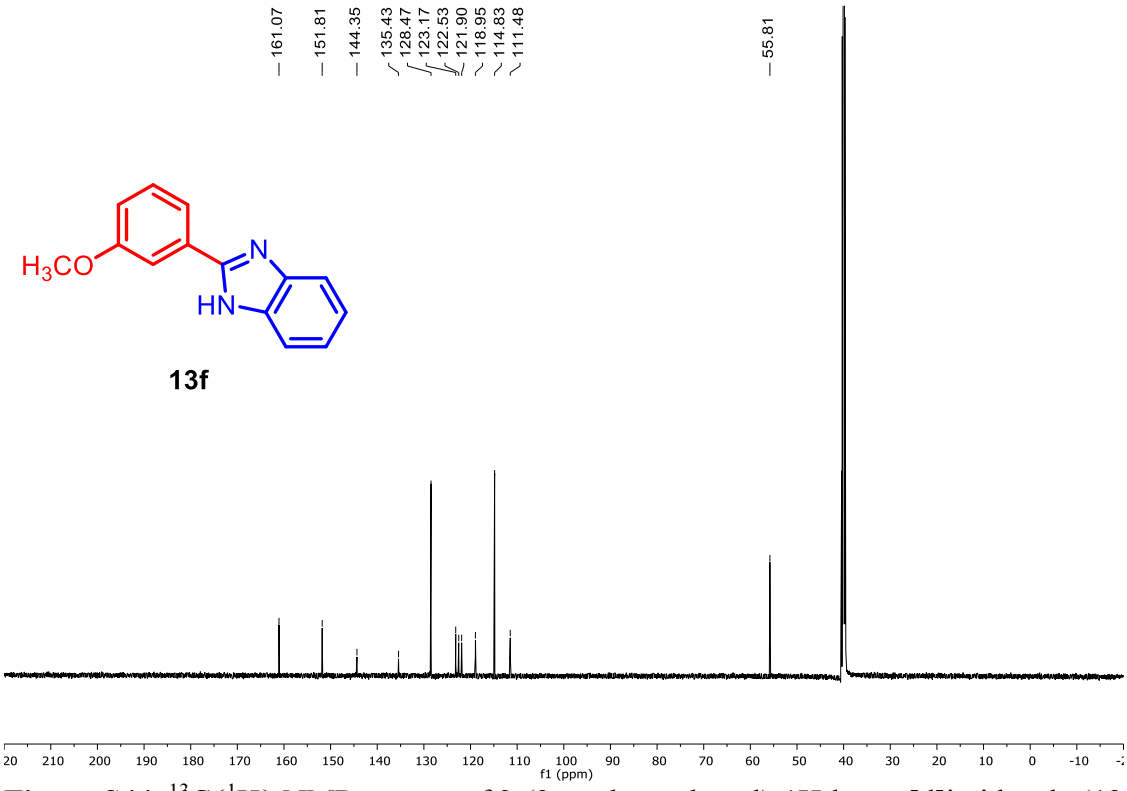

Figure S44. ^{13}C{^{1}H} NMR spectra of 2-(3-methoxyphenyl)-1H-benzo[d]imidazole (**13f**)

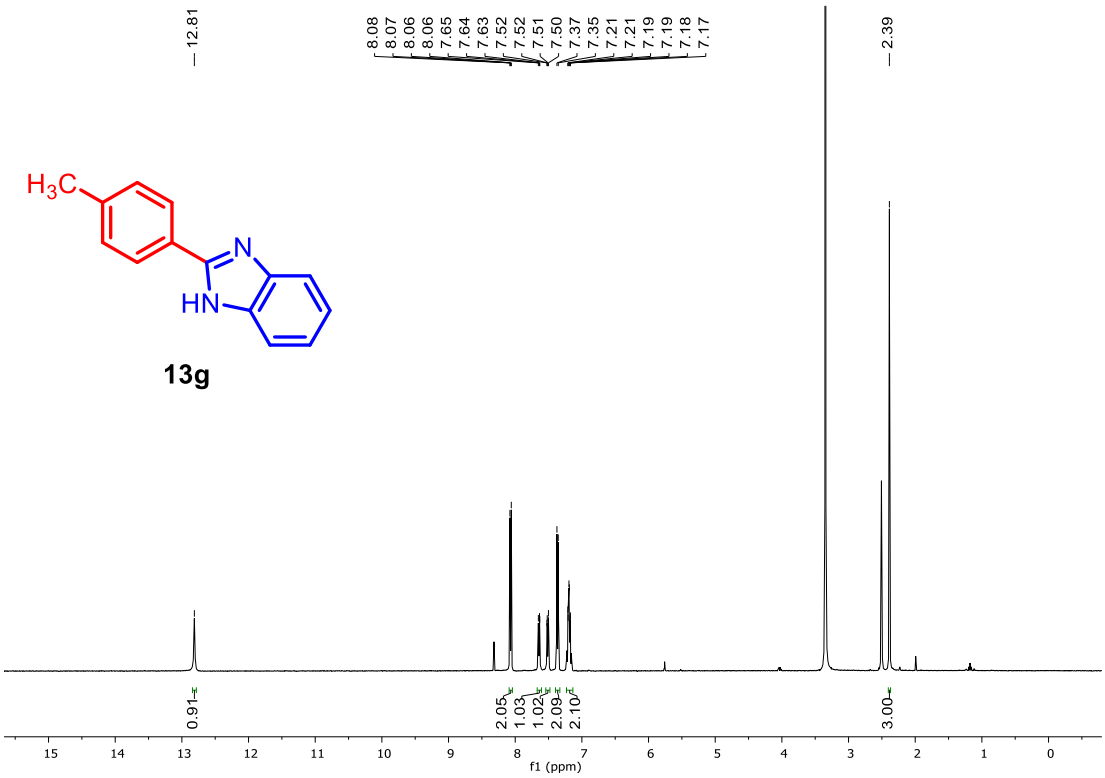

Figure S45. ^{1}H NMR spectra of 2-(p-tolyl)-1H-benzo[d]imidazole (**13g**)

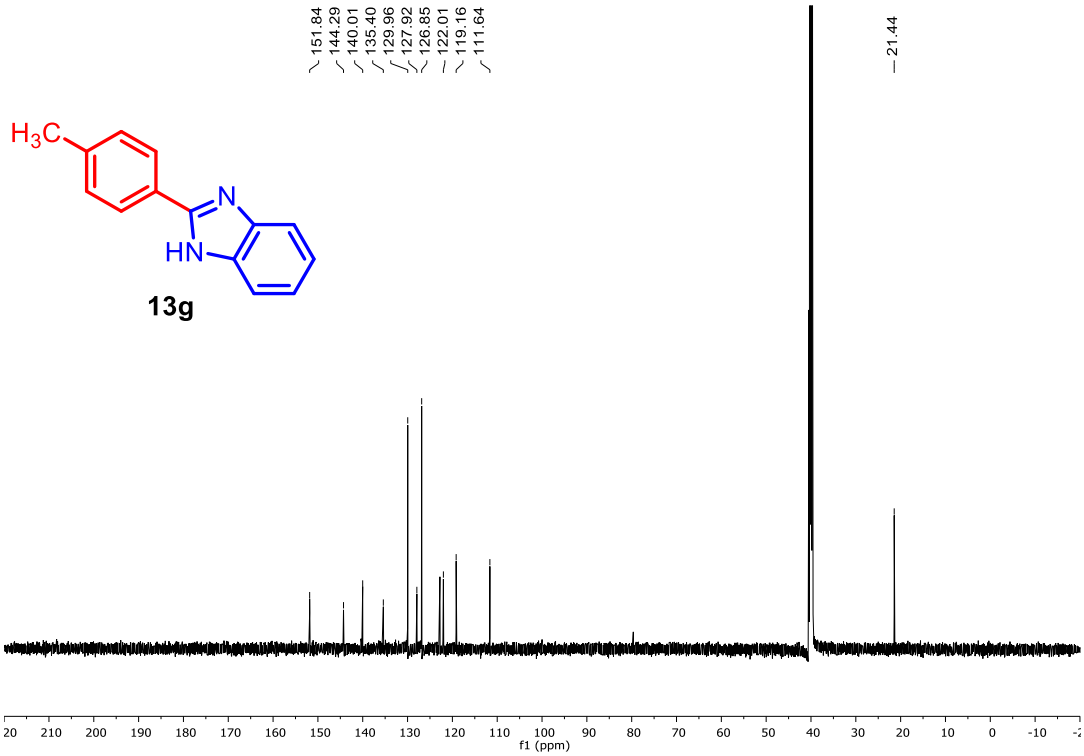

Figure S46. ^{13}C{^{1}H} NMR spectra of 2-(p-tolyl)-1H-benzo[d]imidazole (**13g**)

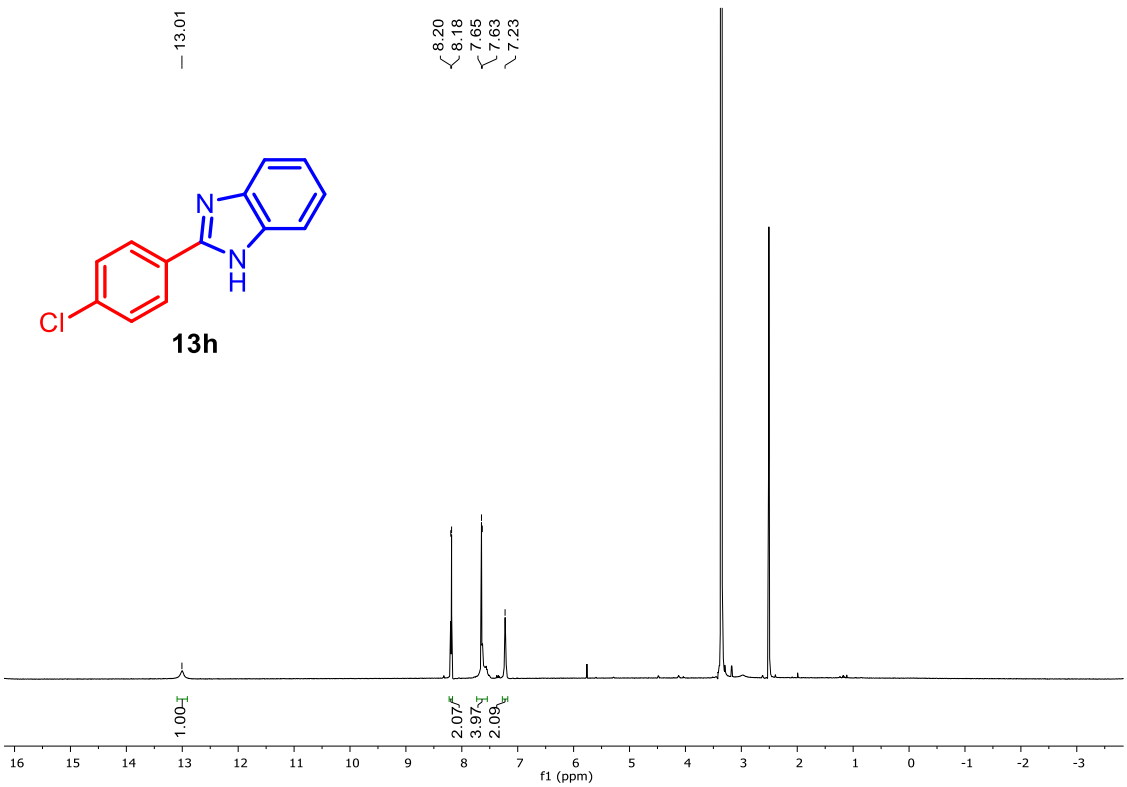

Figure S47. ^{1}H NMR spectra of 2-(4-chlorophenyl)-1H-benzo[d]imidazole (**13h**)

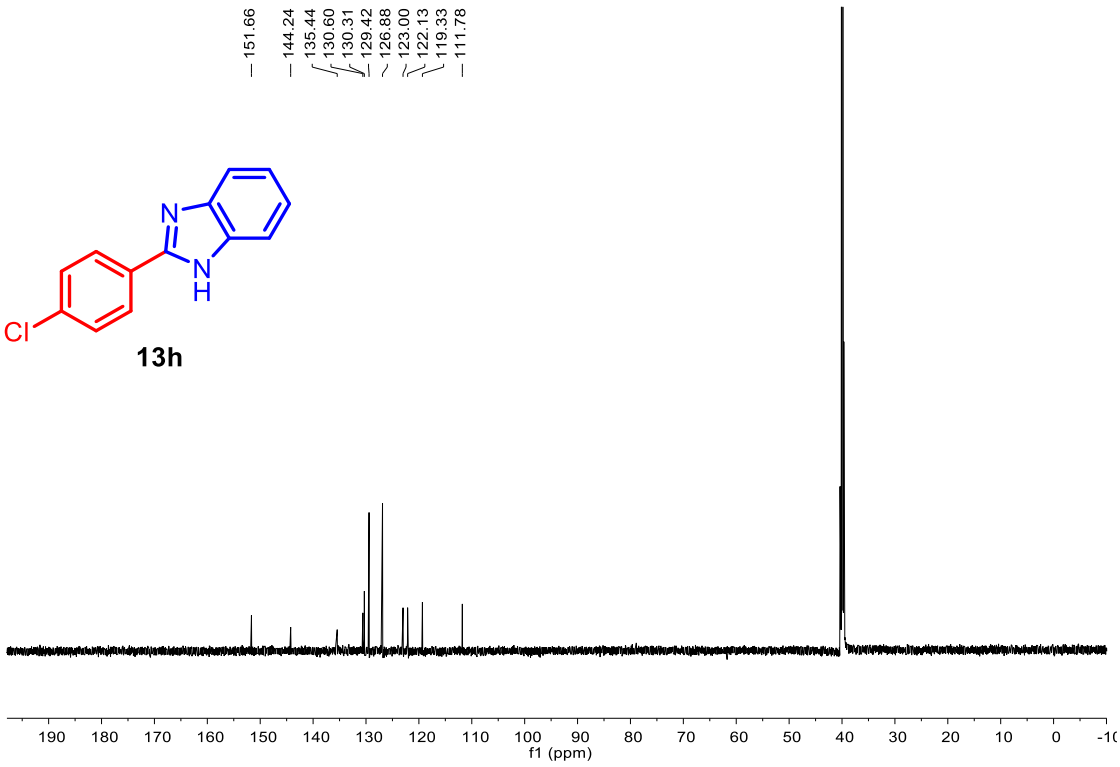

Figure S48. ^{13}C{^{1}H} NMR spectra of 2-(4-chlorophenyl)-1H-benzo[d]imidazole (**13h**)

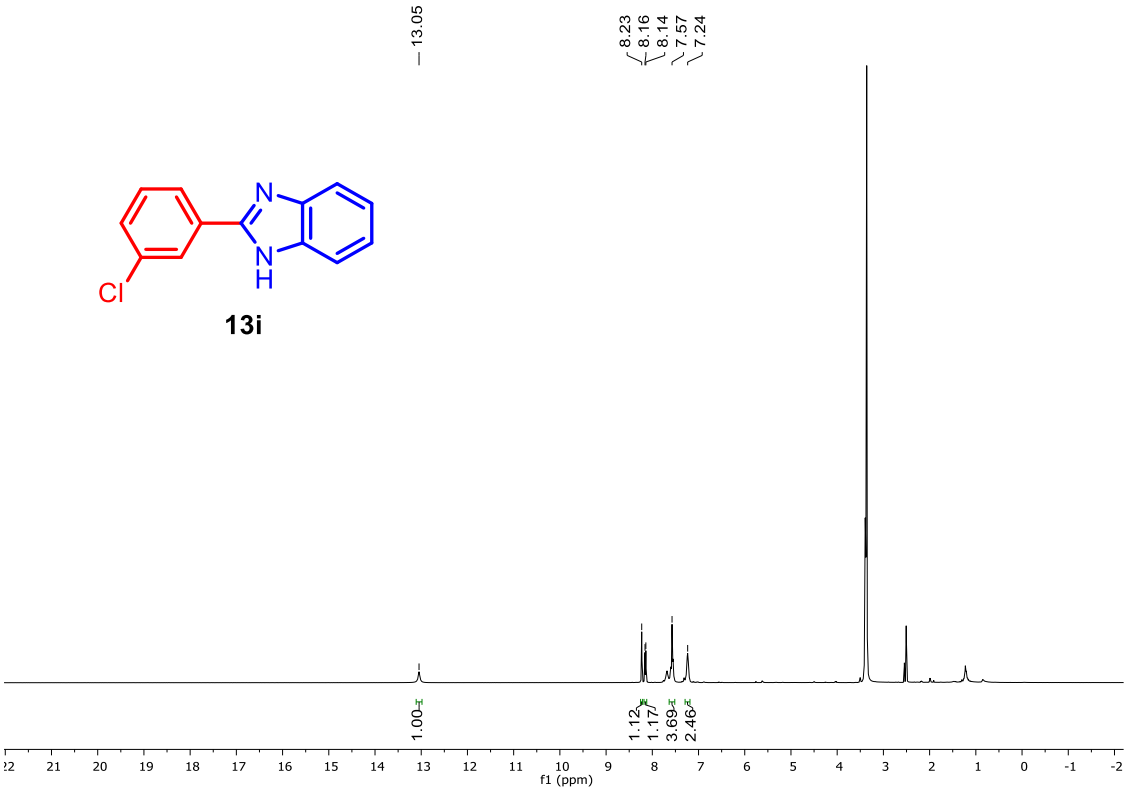

Figure S49. ^{1}H NMR spectra of 2-(3-chlorophenyl)-1H-benzo[d]imidazole (**13i**)

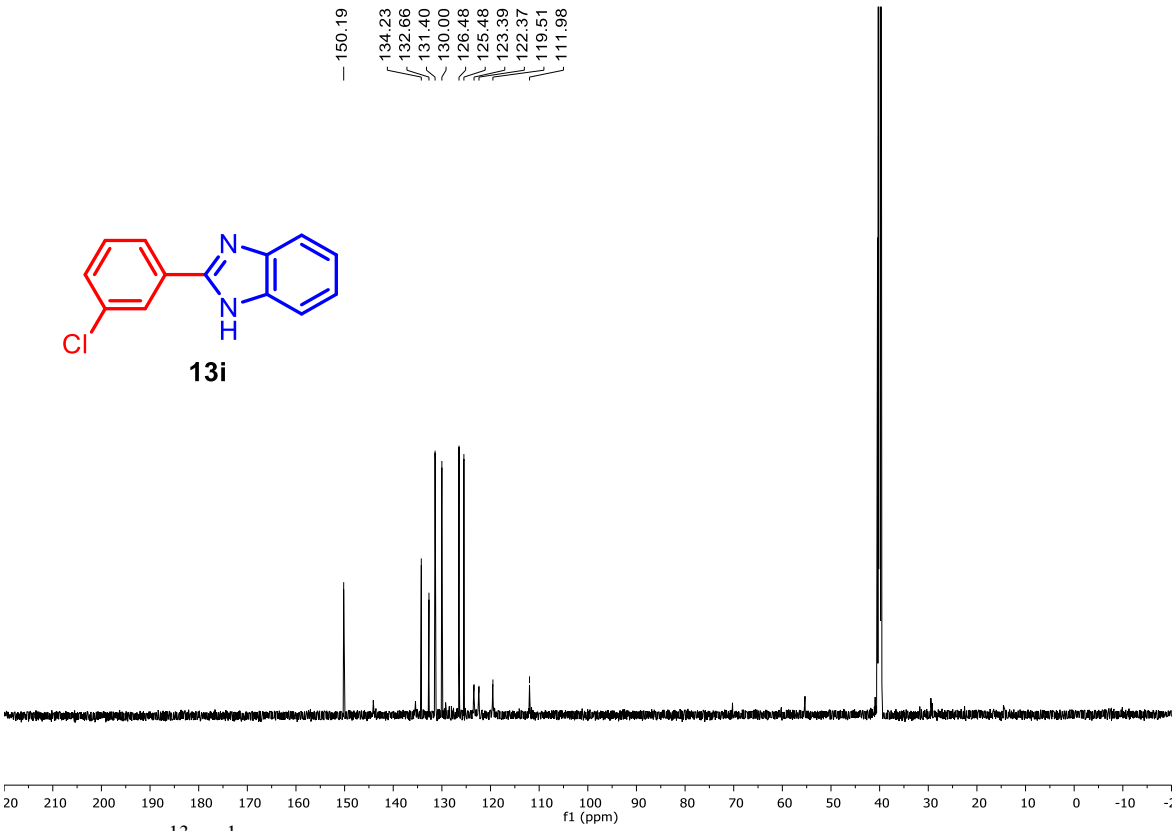

Figure S50. ^{13}C{^{1}H} NMR spectra of 2-(3-chlorophenyl)-1H-benzo[d]imidazole (**13i**)

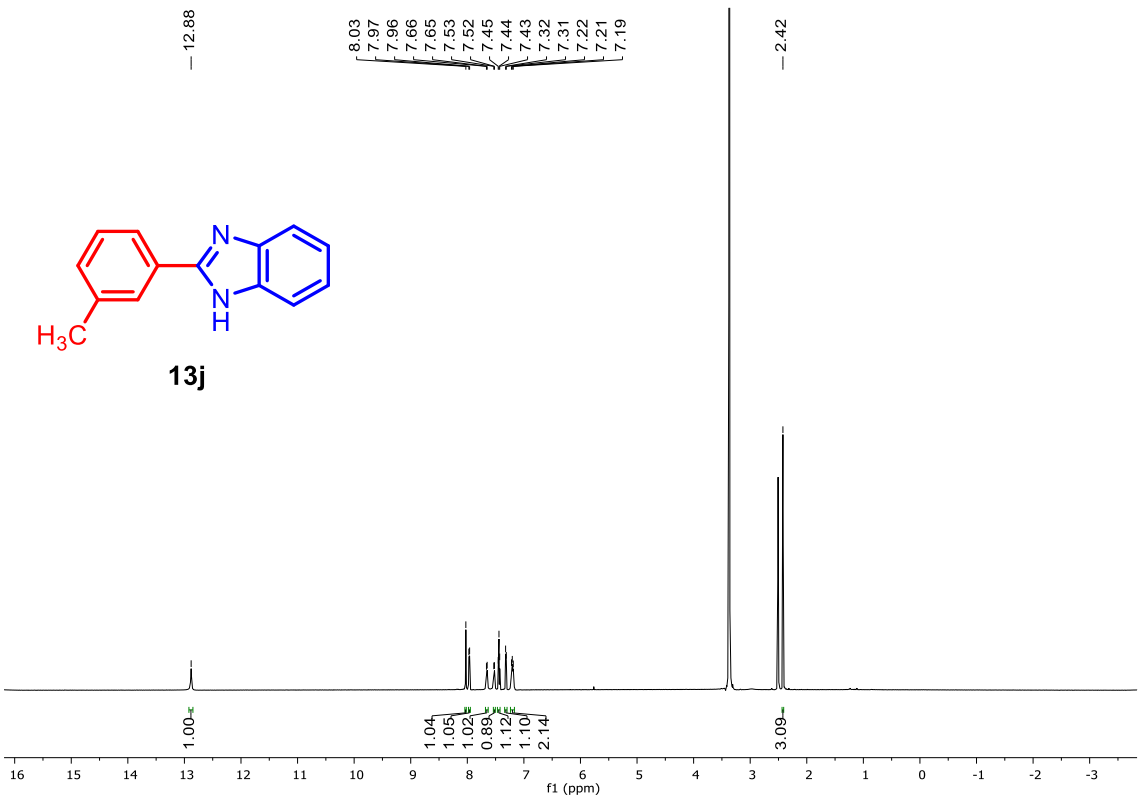

Figure S51. ^{1}H NMR spectra of 2-(m-tolyl)-1H-benzo[d]imidazole (**13j**)

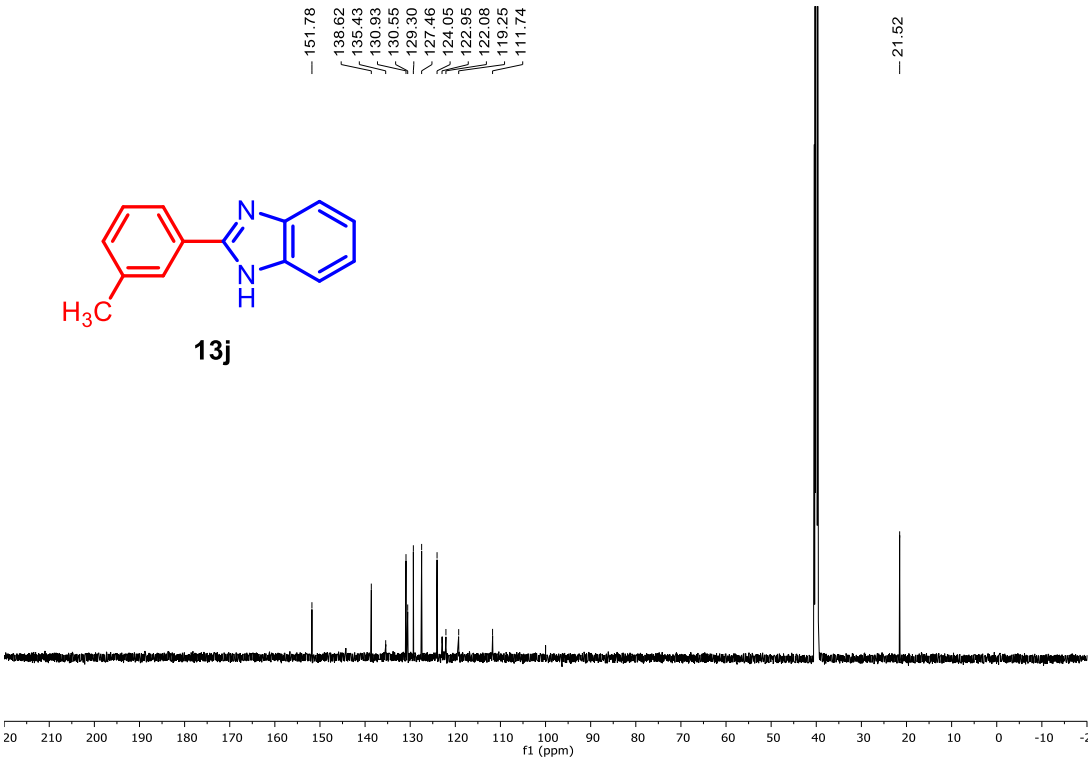

Figure S52. ^{13}C{^{1}H} NMR spectra of 2-(m-tolyl)-1H-benzo[d]imidazole (**13j**)

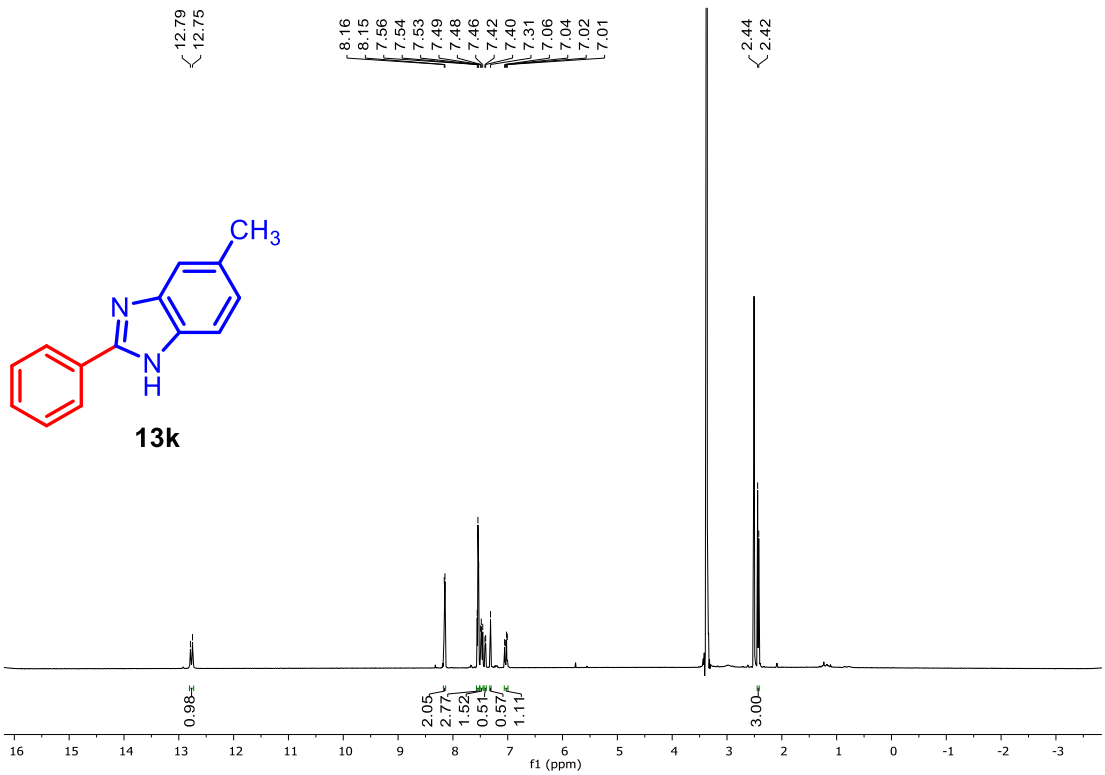

Figure S53. ^{1}H NMR spectra of 5-methyl-2-phenyl-1H-benzo[d]imidazole (**13k**)

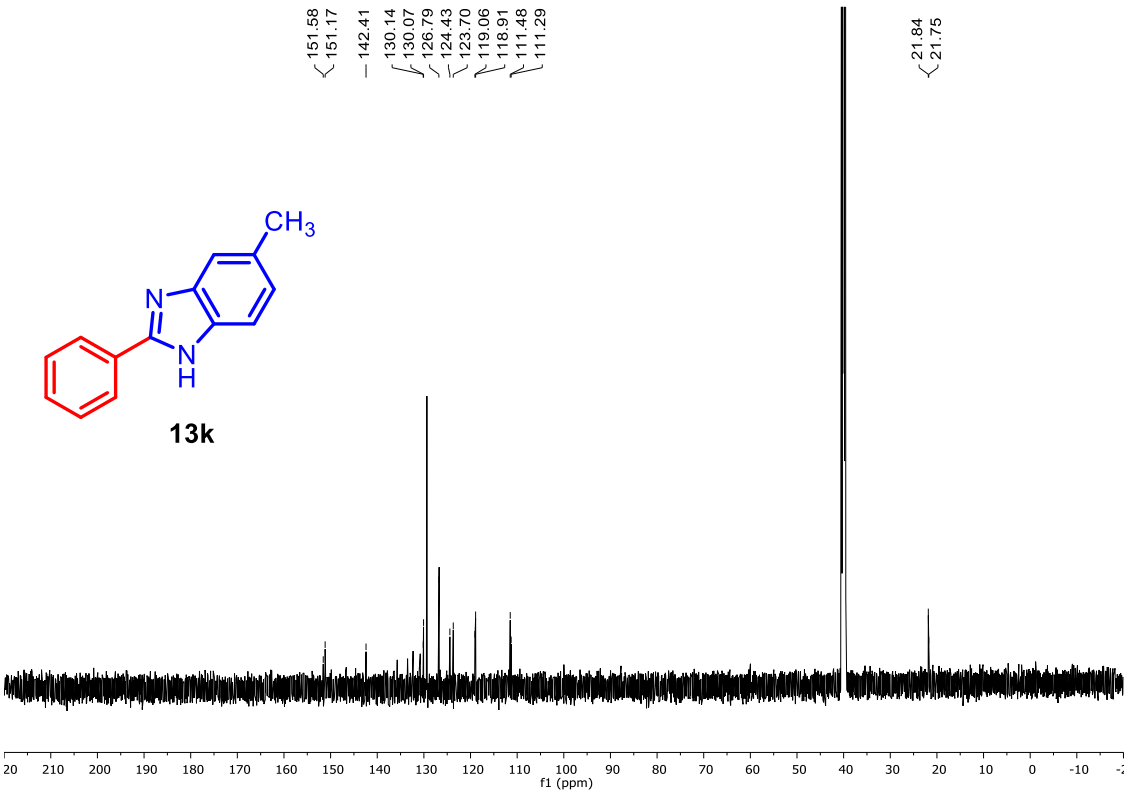

Figure S54. ^{13}C{^{1}H} NMR spectra of 5-methyl-2-phenyl-1H-benzo[d]imidazole (**13k**)

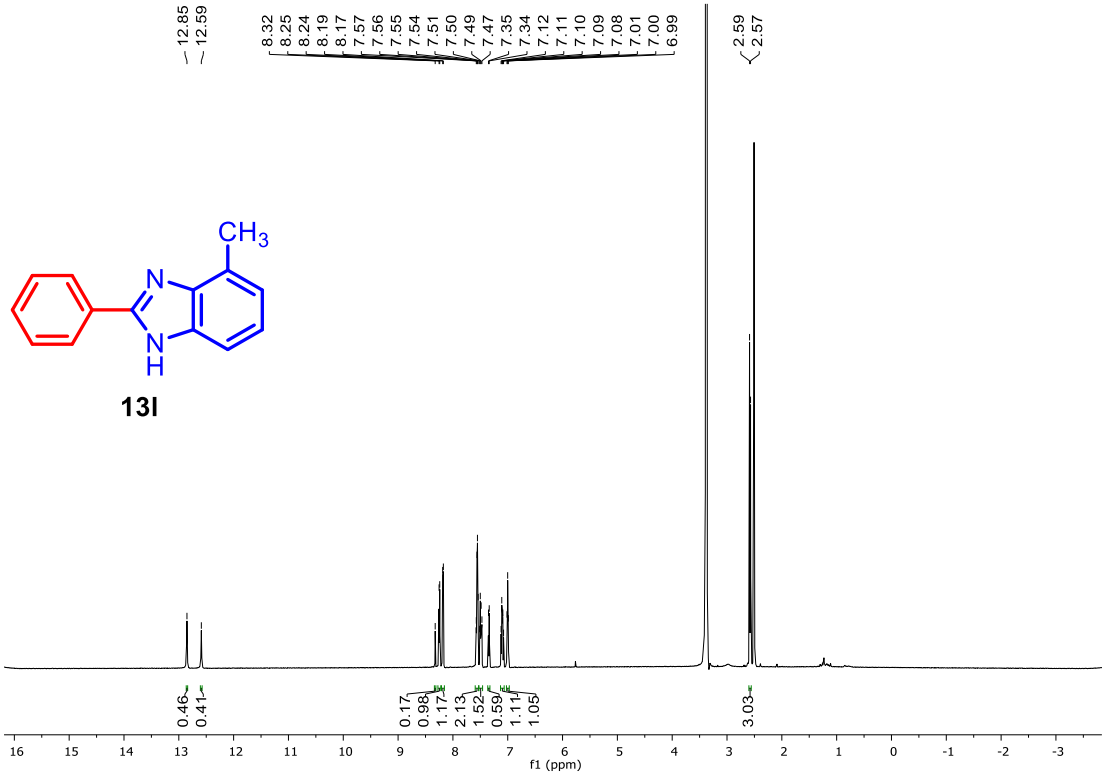

Figure S55. ^{1}H NMR spectra of 6-methyl-2-phenyl-1,4-dihydrocyclopenta[d]imidazole (**13l**)

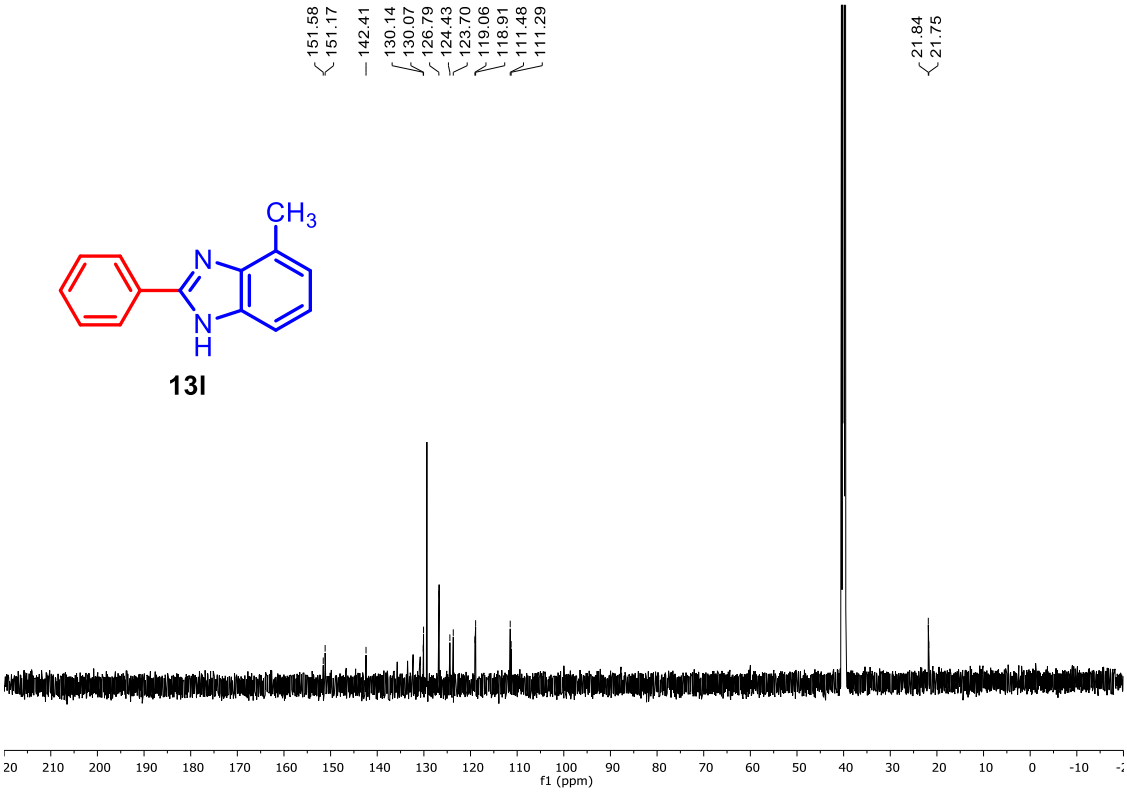

Figure S56. ^{13}C{^{1}H} NMR spectra of 6-methyl-2-phenyl-1,4-dihydrocyclopenta[d]imidazole (**13l**)

3. Computational studies

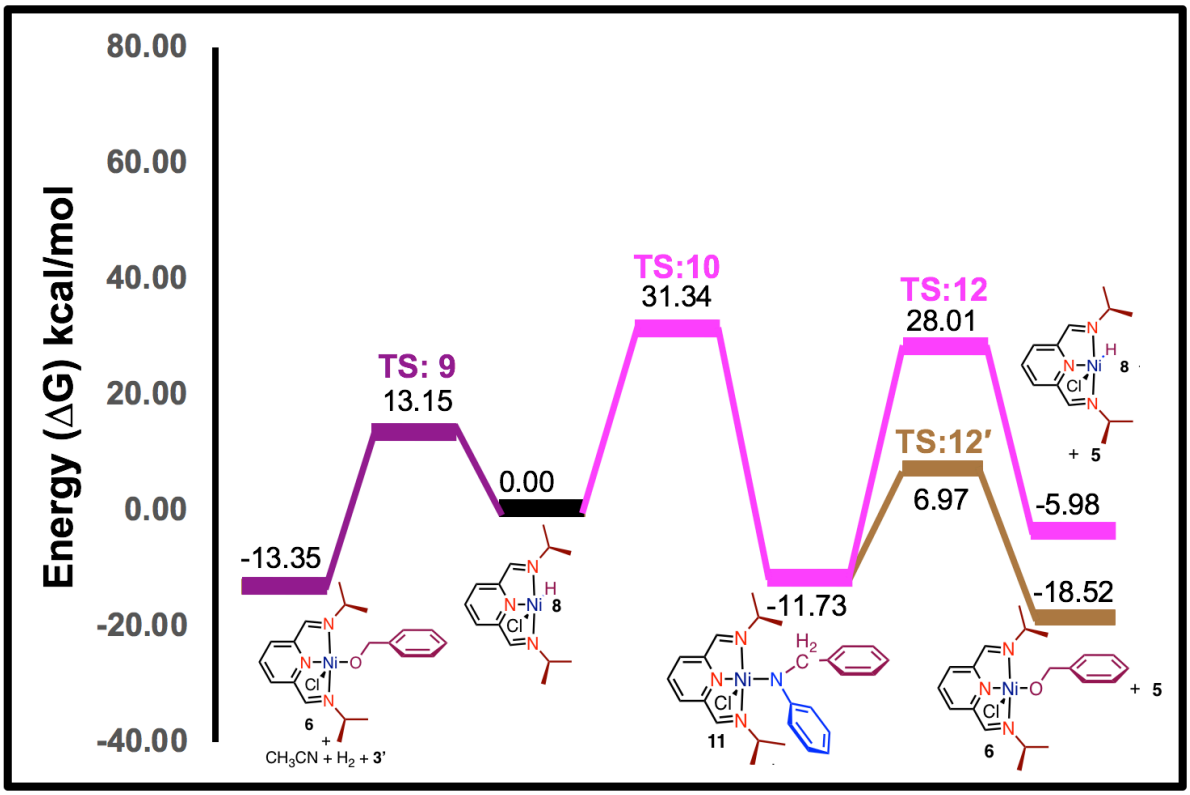

Figure S57. Comparison of free energies of various paths available for **8** and **11**

Table S3: Comparison of relative energy values obtained from optimization without dispersion correction, single-point calculations with dispersion correction and optimization with dispersion correction for the alcoholysis path

M	ΔE(A)	ΔE(B)	ΔE(C)
8 +5'	0.00	0.00	0.00
10	28.20	15.62	14.71
11	-18.24	-30.79	-26.09
11′	-22.83	-43.83	-45.36
12	-15.02	-40.12	-41.71
6 + 5	-37.29	-49.16	-48.05

BS1 = SDD for Ni atom and 6-311G(d) for all other atoms

ΔE = Relative energy values

A = B3LYP/BS1

B = B3LYP/BS1; EmpiricalDispersion=GD3BJ was included using single-point calculations

C = B3LYP/BS1; Geometries were optimized using EmpiricalDispersion=GD3BJ

Table S4: Effect of various dispersion correction methods on the energy profile of the reaction

M	ΔE(A)	ΔE(GD2)	ΔE(GD3)	ΔE(GD3BJ)	ΔE(PFD)
6	0.00	0.00	0.00	0.00	0.00
7	40.31	45.18	45.95	45.50	38.37
8	28.10	38.00	38.26	38.77	41.93
9	39.87	46.18	46.35	46.15	35.39
6 + H2	19.78	25.69	25.98	26.20	41.78
8 +5'	0.00	0.00	0.00	0.00	0.00
10	28.20	16.06	17.14	15.62	7.22
11	-18.24	-31.41	-29.29	-30.79	-35.99
12	8.01	-8.53	-6.89	-9.02	-13.05
8 + 5	-23.48	-29.52	-28.99	-29.32	-28.41
8 +5'	0.00	0.00	0.00	0.00	0.00
10	28.20	16.06	17.14	15.62	7.22
11	-18.24	-31.41	-29.29	-30.79	-35.99
11′	-22.83	-45.17	-42.95	-43.83	-47.70
12	-15.02	-39.72	-38.13	-40.12	-52.76
6 + 5	-37.29	-48.94	-48.54	-49.16	-52.09

BS1 = SDD for Ni atom and 6-311G(d) for all other atoms

ΔE = Relative energy values

A = B3LYP/BS1

GD2 = B3LYP/BS1; EmpiricalDispersion=GD2

GD3 = B3LYP/BS1; EmpiricalDispersion=GD3

GD3BJ = B3LYP/BS1; EmpiricalDispersion=GD3BJ

PFD = B3LYP/BS1; EmpiricalDispersion=PFD

All the dispersion corrections were included on the basis of single point calculations at optimization level (A)

Table S5: Effect of various DFT methods and basis sets on the energy profile of the reaction

M	ΔE(A)	ΔE(B)	ΔE(C)	ΔE(D)	ΔE(E)	ΔE(F)	ΔE(G)
6	0.00	0.00	0.00	0.00	0.00	0.00	0.00
7	40.31	39.67	38.71	37.98	40.25	39.18	44.86
8	28.10	26.82	27.27	23.44	33.44	26.22	37.49
9	39.87	40.60	40.91	38.90	45.18	39.99	46.88
6 + H2	19.78	22.66	24.47	24.95	29.12	22.25	29.07
8 +5'	0.00	0.00	0.00	0.00	0.00	0.00	0.00
10	28.20	27.84	25.30	25.17	17.27	28.95	15.26
11	-18.24	-18.60	-21.76	-19.39	-29.30	-16.56	-31.15
12	8.01	6.72	2.47	4.88	-9.14	8.81	-10.31
8 + 5	-23.48	-24.55	-27.49	-26.45	-31.00	-23.80	-30.38
8 +5'	0.00	0.00	0.00	0.00	0.00	0.00	0.00
10	28.20	27.84	25.30	25.17	17.27	28.95	15.26
11	-18.24	-18.60	-21.76	-19.39	-29.30	-16.56	-31.15
11′	-22.83	-20.99	-23.15	-21.40	-38.71	-19.43	-42.00
12	-15.02	-12.43	-15.33	-12.09	-33.18	-9.88	-37.52
6 + 5	-37.29	-33.16	-33.99	-30.28	-41.84	-32.50	-45.03

BS1 = SDD for Ni atom and 6-311G(d) for all other atoms
BS2 = SDD for Ni atom and 6-311++G(d,p) for all other atoms
BS3 = SDD for Ni atom and cc-PvTZ for all other atoms
ΔE = Relative energy values
A = B3LYP/BS1
B = B3LYP/BS2//B3LYP/BS1
C = B3PW91/BS2//B3LYP/BS1
D = PBEPBE/BS2//B3LYP/BS1
E = M06/BS2//B3LYP/BS1
F = B3LYP/BS3//B3LYP/BS1
G = B3LYP/BS2//B3LYP/BS1; EmpiricalDispersion=GD3BJ[#]

All the calculations were performed in gas phase to match the experimental conditions. [#]Dispersion corrections were included on the basis of single point calculations.

4. Gas Chromatography analysis. GC analysis (TCD detection) was performed on a Agilent 7820-GC instrument fitted with Agilent Front SS7 inlet N2 HP5 column (30 m length x 0.32 mm ID) using the following method:

Agilent 7820-GC Detector

Oven temperature 70 °C

Time at starting temp: 0 min

Hold time = 10 min

Flow rate (carrier): 5 mL/min (N2)

Split ration: 50

Inlet temperature: 70 °C

Detector temperature: 250 °C

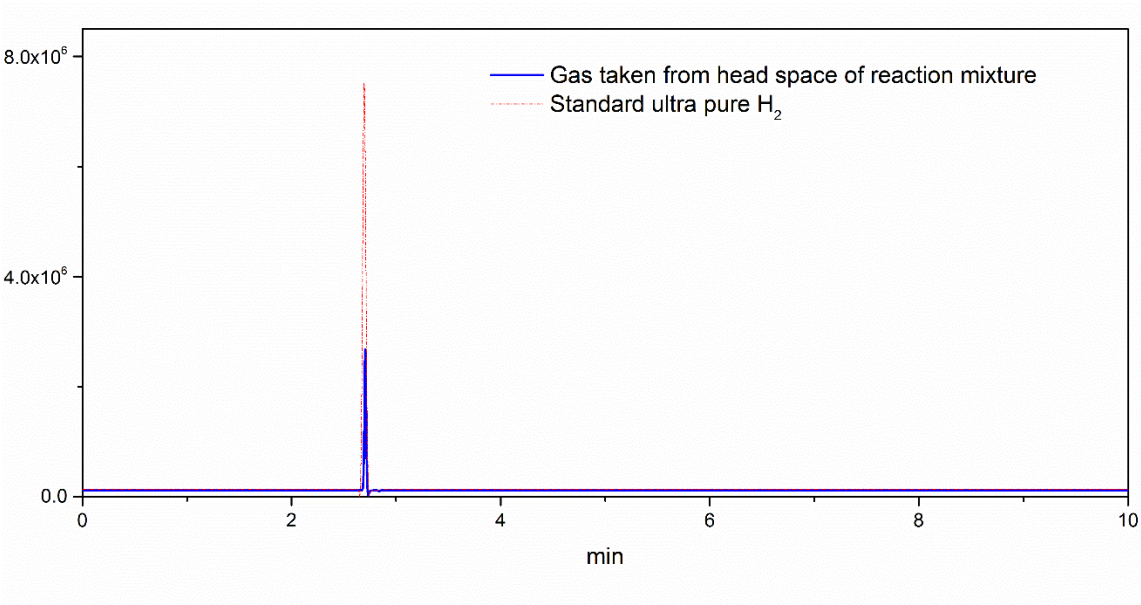

Figure S58. Evidence for H2 evolution in the reaction of **2** catalyzed dehydrogenation of **3** at 140 °C via GC analysis.

4. HRMS analysis.

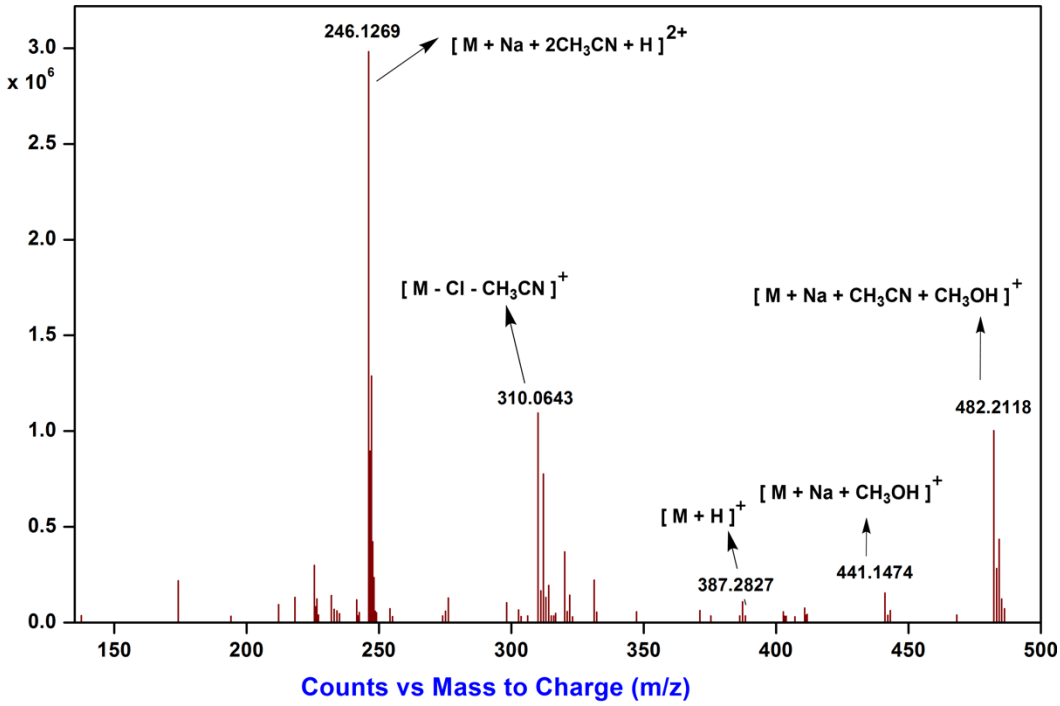

Figure S59. HRMS (ESI) Plot of complex **2**.

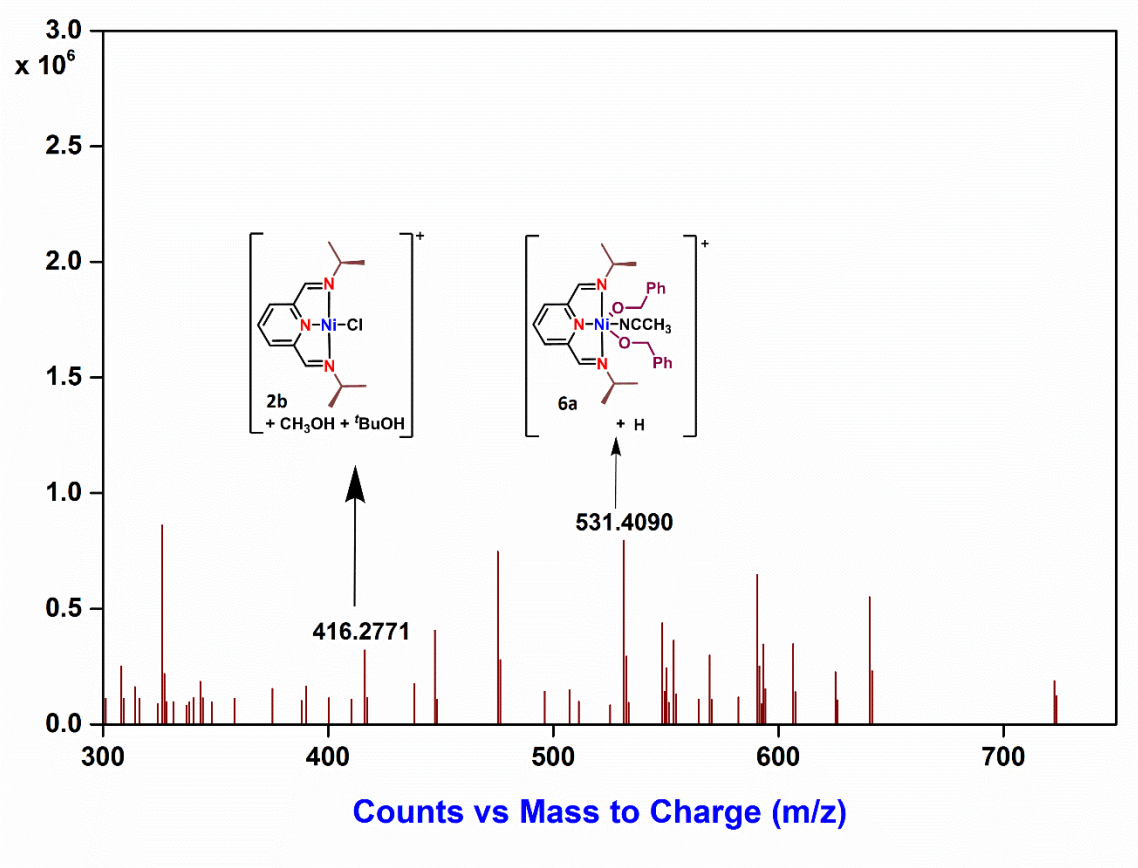

Figure S60. HRMS (ESI) Plot of the Reaction Mixture at 0 hr.

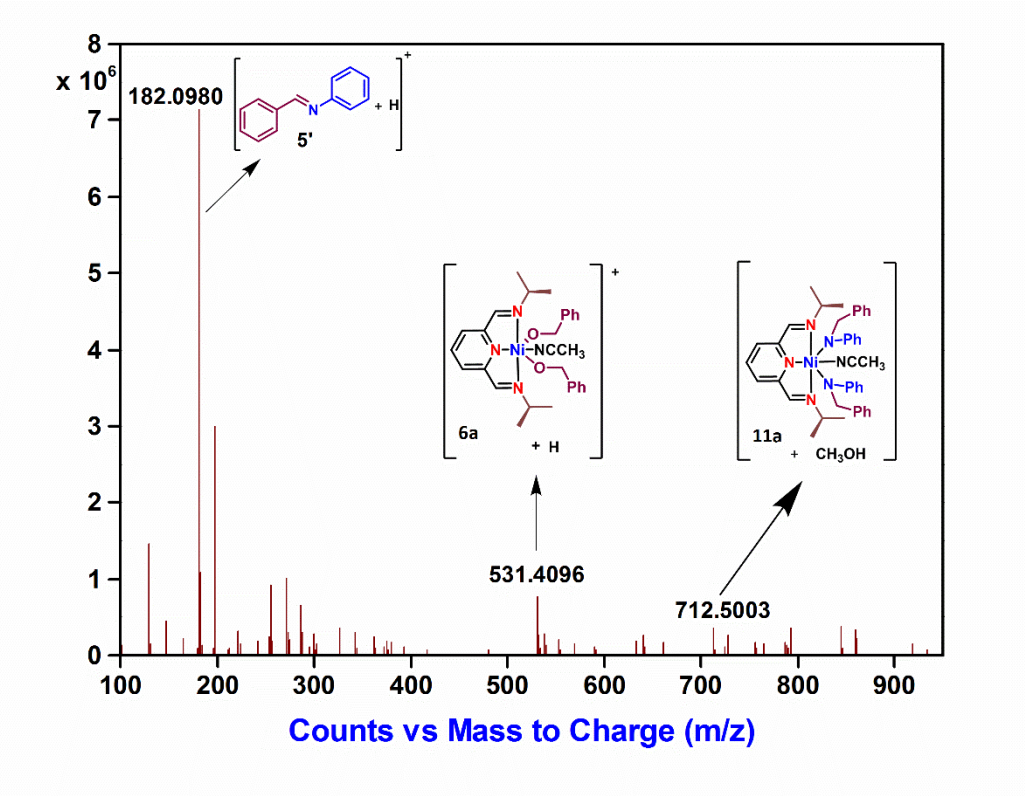

Figure S61. HRMS (ESI) Plot of the Reaction Mixture at 4 hr.

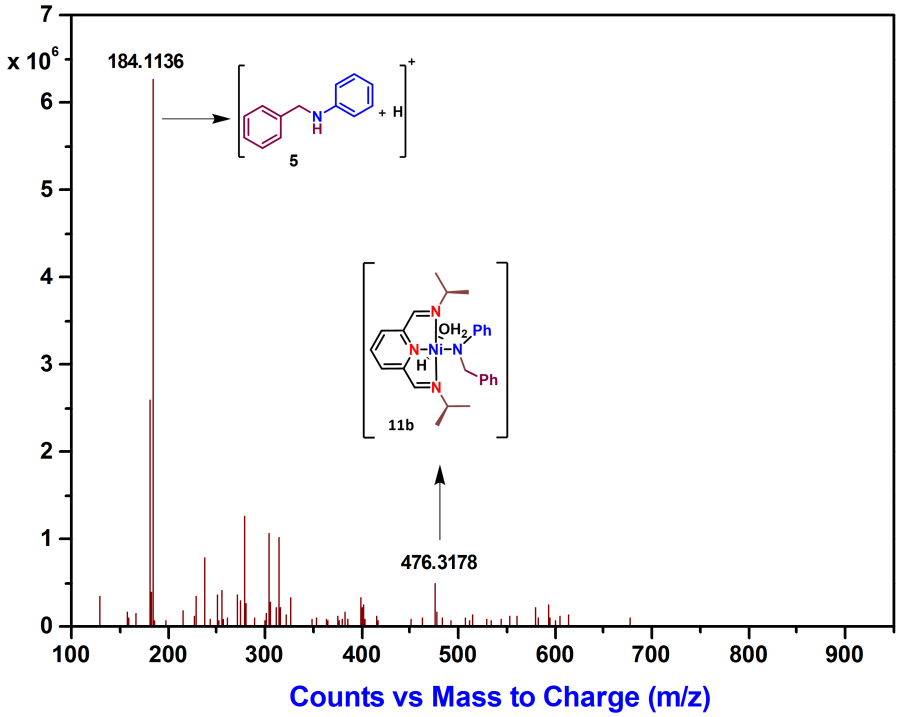

Figure S62. HRMS (ESI) Plot of the Reaction Mixture at 72 hr

6. EPR analysis

The X-band EPR spectra were recorded on a JES-FA200 ESR spectrometer, at room temperature with microwave power of 0.998 mW and microwave frequency of 9.14 GHz.

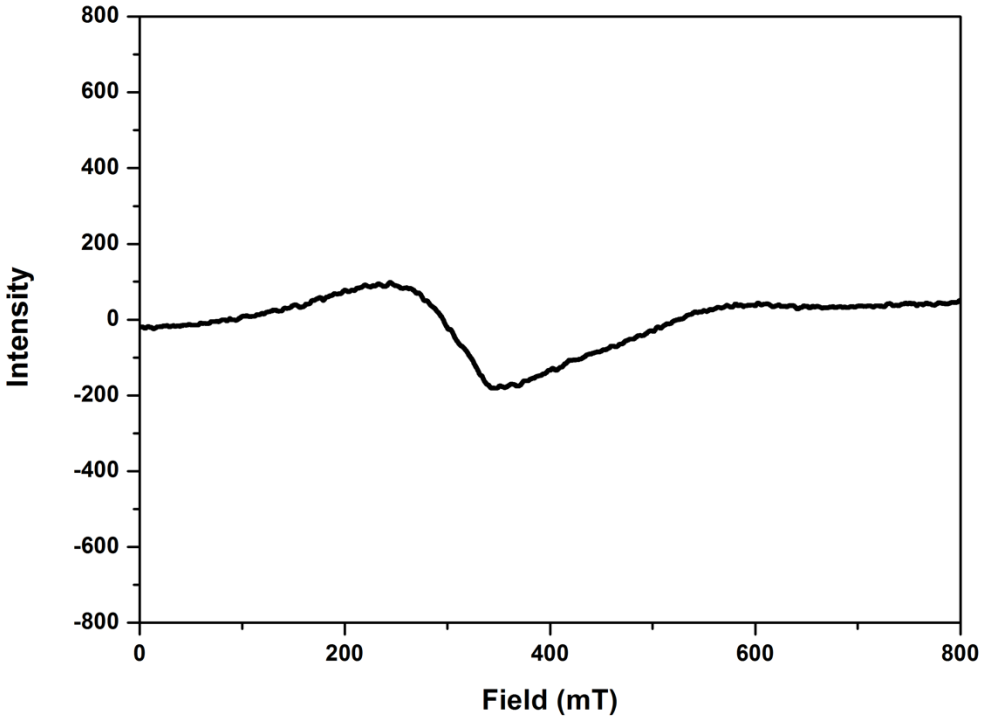

Figure S63. EPR spectrum of complex **2**(g = 2.28).